POAC'15
Trondheim, Norway

Proceedings of the 23rd International Conference on
Port and Ocean Engineering under Arctic Conditions
June 14-18, 2015
Trondheim, Norway

FULL SCALE ACTIONS FROM FIRST YEAR RIDGE INTERACTIONS WITH FIXED STRUCTURES

Åse Ervik[1]
[1]Centre for Sustainable Arctic Marine and Coastal Technology, Norwegian University of Science and Technology, Trondheim, Norway

ABSTRACT

The objective of this paper was to study full scale actions from first year ice ridges on fixed structures. The first part is a review of reported full scale global loads and associated failure modes from ice ridges compared to level ice, on three fixed structures. The instrumented structures are the Molikpaq, the piers of the Confederation Bridge and Nordströmgrund lighthouse. The highest ridge loads on Nordströmgrund lighthouse and the piers of the Confederation Bridge were associated with crushing and combined crushing/bending respectively. On Molikpaq crushing of first year ridges was not reported. In the second part of this paper data is analyzed. A limit force analysis was performed to estimate a critical ice ridge length of approximately 9km for crushing to occur on the Molikpaq compared to 20m on Nordströmgrund lighthouse. Accordingly some Nordströmgrund data were analyzed to compare global loads derived from load panels and tilt. A ratio between panel load and tilt was found for a quasi-static 5m deep ridge interaction with the instrumented side of the lighthouse. For the ridge a ratio of 8.2 kN/μradians was derived, compared to 12kN/μradians for level ice both ratios without uncertainties. The different ratio indicates that load panels underestimate ridge keel loads. The analysis also showed that it is not possible to obtain a unique ratio between global load and tilt for ridges, due to the stiff bottom foundation that makes the tilt sensitive to changes in point of action i.e. ridge keel depth.

INTRODUCTION

Actions from ice ridges is assumed to establish dimensioning loads on infrastructure and offshore installations in ice-infested areas, when icebergs are not present. In the past decades great effort has been put into predicting ice ridge loads. A study by Timco and Croasdale (2006) shows that ice ridge loads on a vertical structure predicted by twenty-one ice experts ranged with a factor of five. The study shows that research on ice ridge structure interactions is still needed. This paper begins with a review of full scale first year ice ridge loads on three instrumented fixed structures. The structures are the Molikpaq (CAN), the piers of the Confederation Bridge (CAN) and the Nordströmgrund Lighthouse (SWE). The purpose is to investigate ice ridge load levels and associated failure modes compared to level ice, measured on fixed structures.

The second part of this paper is an analysis of some ridge interaction data. Global loads derived from load panels and tilt are compared, for this analysis data from Nordströmsgrund lighthouse are used. Finally a limit force analysis is performed to compare the minimum ice ridge length for crushing to occur on the three structures.

Structure geometry, instrumentation and location

Ice actions depend on the type of interaction. In the following the three structure geometries, instrumentations and locations are presented. Nordströmgrund lighthouse is a vertical structure and Molikpaq is close to vertical. The piers of the Confederation Bridge on the other hand are conical which favors breaking of ice in bending. Both Nordströmgrund lighthouse and the Confederation Bridge piers are narrow structures while the Molikpaq is a wide structure (Table 1). All the structures are fixed to the sea bed in the bottom foundation, but free to rotate and deflect in all other parts limited by the structure stiffness.

Table 1. Some key structure and location parameters

	Molikpaq	Confederation Bridge	Nordströmgrund Lighthouse
Structure width (MWL) [m]	90	14.2	7.6
Incliation (MWL) [°]	82	52	90
Dominant ice drift dir.	NE	NW (SE tides)	NE

*MWL mean water level

Full scale data is obtained by instrumenting the structures with load panels, accelerometers, tiltmeters, optic sensors (laser, EM, ULS) and video coverage. In addition weather data and dairies are documented. Global loads on the Molikpaq and Nordströmgrund lighthouse were found by load panels (Timco et al., 2000),(Bjerkås, 2006) , tiltmeters were used to find global loads on the Confederation bridge piers after 2003 when load panels broke (Brown, 2007).

In addition to measuring load and responses some ice parameters were measured. At Molikpaq ice velocities and ice ridge sails were estimated from videos. At Nordströmgrund ice velocities and direction were estimated form videos, wind speed/directions and air temperatures by a weather station. Ice thickness above water was found with laser, below water an electromagnetic device (EM) was used. For ridge keels EM footprint data is too coarse, an upward looking sonar (ULS) gives more precise ridge profiles. At Nordströmgrund a ULS was installed in 2000 but broke early in 2001. Based on linear regression between available ULS and EM data at Nordströmgrund; maximum keel depths from ULS was approximately 3 times the EM maximum (Bjerkås, 2006). At the Confederation bridge a weather station records wind speed/direction and air temperatures. Since the Confederation Bridge is 13km long; wind loads must be subtracted from tilt measurements to find ice loads. Ice drift speeds were measured by an acoustic doppler current profiler and ice thickness is measured with ULS.

Molikpaq was (1984-1986) located in the Beaufort Sea, experiencing heavy ice conditions including old ice features. The Confederation Bridge crosses the Northumberland Strait in Canada and the Nordströmgrund lighthouse is located outside Luleå in Sweden, both are located in temperate areas only experiencing first-year ice features. Based on this; loads from first-year ice ridges were expected to be dimensioning, at least for the temperate structures. Location of the structures are shown in Figure 1.

Classification of ice features

In this paper actions from ice ridges and level ice are compared. WMO (1970) classify ice as either deformed or undeformed, where undeformed ice is level ice while deformed ice is

Table 2. Instrumentation and monitoring, Molikpaq; Timco et al. (2000) and Timco et al. (2005), Confederation Bridge; Brown et al. (2009), Brown (2001), Nordströmgrund lighthouse; Bjerkås (2006) and Schwarz and Jochmann (2001)

	Molikpaq	Confederation Bridge	Nordströmgrund Lighthouse
Load panels	yes (1984-86)	yes (1997-2003)	yes (1987-1989) (1998-2003)
Location panels	SE, E, NE, N	NW	NE, E
Max panel depth [m]	3/6m	2m	1.5m
Response measurements	4 16 (12th April 1986) Extensometer and 10 strain gauges (1984-86)	Tiltmeters, accelerometers	Tiltmeters (1986) (2003), accelerometers (1973-1989) (2001-2003)
Video	yes (1984-86)	yes (1997-)	yes (1979) (2001-2003)
Other instruments	-	upward looking sonar (ULS) (1997-), Acoustic Doppler Current Profiler (1999-2000)	Laser, electromagnetic device(EM) (2001-2003), ULS (2000-2001)

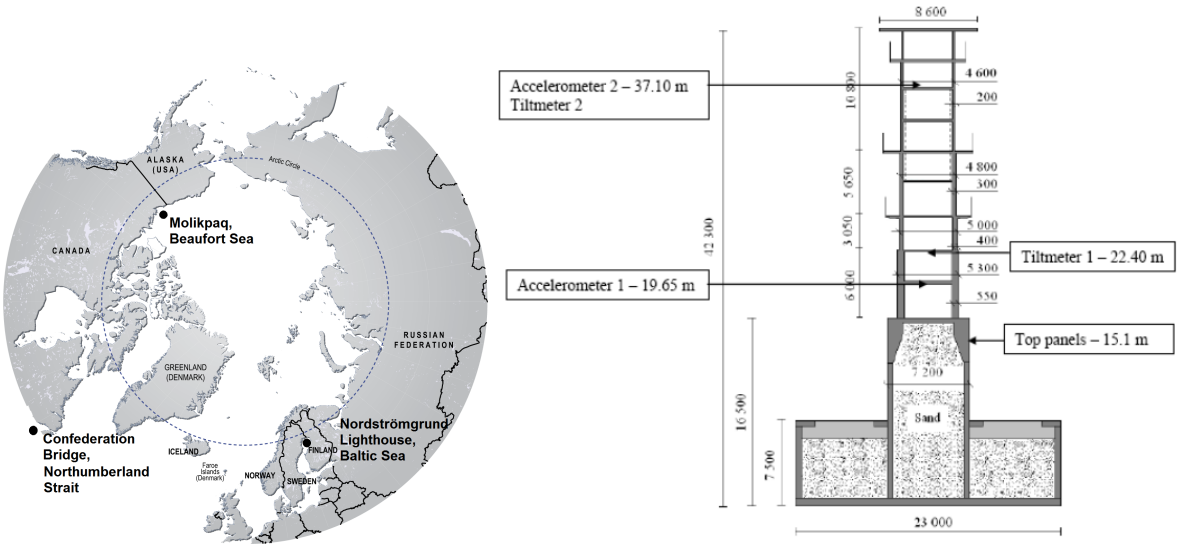

Figure 1. To the left:Map showing the location of the Molikpaq, the Confederation Bridge and the Nordströmgrund lighthouse (Ahlenius, 2005). To the right: Nordströmgrund lighthouse (1998-2003) Bjerkås et al. (2013).

both rafter and ridged ice. Level ice is thermally grown ice. When visually studying ice it

is seldom possible to distinguish level ice from rafted ice, therefore ice thickness should be measured manually and compared to thermodynamic estimates in order to distinguish between undeformed and deformed ice.

Limit scenarios and failure modes

It is important to distinguished between load limiting mechanisms and failure modes. There are three recognized load limiting mechanisms. They are limit stress, limit force and limit momentum. Ice load is limited by stress when ice fails directly against the structure (in crushing, bending, buckling, creep or shear), this requires sufficient driving forces. If the driving forces from the wind and current are insufficient to fail the ice or if inhomogeneities in ice sheet causes the ice to fail adjacent to the structure surface; driving forces limits the ice load i.e. a limit force mechanism. If the momentum of the ice is insufficient the ice will come to halt and the ice load is limited by momentum or energy.

The mode of which the ice fails against the structure controls the load level. Recognized failure modes are crushing, bending, creep, buckling, splitting and spalling (ISO19906, 2010). For ridges other failure modes are also reported such as ridge spine failure, failure behind the ridge (Timco et al., 2000) and dodging (Kärna and Jochmann, 2004). The dodging failure was described for a ridge with a sail hight of 2m on the 1st of April 2002 (Kärna and Jochmann, 2004):"Instead of a ridge penetration, the drift direction changed for a while. Then the structure found the boundary between the level ice and the rafted ice.". Timco et al. (2000) and Bjerkås (2006) also differ between local and global failures. Where local failures occur continuously over the whole structure width while global failures occur on a concentrated part of the structure. The failure mode that produces the highest load is crushing since the crushing strength is generally the highest strength in sea ice.

REVIEW OF GLOBAL LOADS AND FAILURE MODES

Failure modes and global loads both dependent on structure geometry and ice parameters; when designing the Confederation bridge between 20 and 25 parameters were used to find design ice loads (Brown et al., 2009). Table 3 gives a summary of maximum loads and failure modes of ridges compared to level ice.

The maximum reported first year ridge load on Molikpaq was 89MN associated with a global failure behind the ice ridge. On Molikpaq crushing of first year ridges was not observed. For level ice the maximum global load found was 131MN. The level ice failure mode was unknown, but the second largest level ice load (110MN) was caused by crushing of level ice with a thickness of 1.2m (Timco and Johnston, 2004). Molikpaq, being in the Arctic, encountered old ice features in addition to first year ice, crushing of level old ice produced the overall highest loads up to 466MN. Wright (1986) reports that strong dynamic vibrations were sometime associated with crushing of old ice features.

Some of the Nordstömgrund data are not yet analyzed, but the highest ridge load reported until today is 3MN occurred during crushing of a ridge of 9m depth. During the interaction the ice velocity decreased to zero and dynamic accelerations up to $1m/s^2$ were registered. The largest quasi-static ridge load reported is 1.3MN for crushing of a ridge keel of 6m (Bjerkås, 2006). The highest level ice load reported to this date is 3.5MN measured during crushing of level ice with dynamic accelerations up to $2m/s^2$ (Bjerkås et al., 2013). For large ice ridges dodging was sometimes reported at Nordströmgrund lighthouse. In Figure 2 the full time series

from 30th of March is shown, a dodging event is seen from 18.00-19:30. For large ice ridges limiting mechanisms seems to be important, it is stressed that a comprehensive study of all Nordströmgrund data is not yet done, and should be carried out to validate what caused extreme loads.

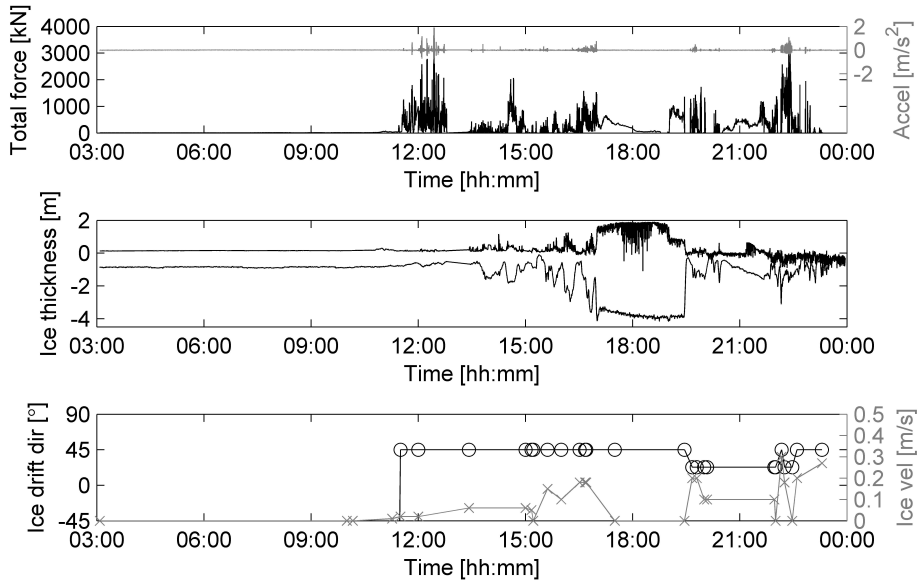

Figure 2. Extreme events from the 30th of March including dodging of and ice ridge. In the bottom plot x marks ice drift velocity and o marks ice drift direction.

Brown et al. (2009) reported the highest ice loads and associated failure modes measured until 2009 on the two center piers of the 13km long Confederation Bridge. The highest ridge load measured was 8.3MN associated with a continuous failure. The failure seemed to be a combination of crushing and bending. The highest level ice load was 8.9MN also associated with a combination of bending and crushing failure.

ANALYSIS AND DISCUSSION

In the second part of this paper some data are analyzed, first an attempt is made to compare panel loads to tilt measured at Nordströmgrund for a quasi-static ice ridge event. This is done in an attempt to investigate if tilt can be used to obtain global ice ridge loads. Accordingly limit ridge building forces are applied to estimate the critical ridge lengths for limit stress to occur on the three structures.

Analyses of tilt and panel loads on Nordströmgrund lighthouse

Global loads on Nordströmgrund lighthouse were originally derived from load panels. Loads from level ice heading from east would be captured by load panels fixed on the N-SE of the lighthouse reaching 1.5m below mean water level (MWL). However, load panels are not capable of obtaining total loads from ridges which reach deeper than 1.5m below MWL.

Frederking (2005) calibrated tilt data from a quasi-static level ice event with heading from the east, he found a ratio between global load and tilt of 12kN/μradians. Arguing that once

Table 3. Full-scale actions from first year ice features. Highest load reported from first year ice ridge (F_{MaxR}) compared to highest overall load reported from first year ice (F_E) .

Maximum ice ridge event	Molikpaq (Timco et al., 2000)	Confederation Bridge (Brown et al., 2009)	Nordströmgrund (STRICE data 2002, Bjerkås (2006))
Date/time [dd.mm.yyyy/hr.min]	NA	29.02.2008/09.29	30.03.2003/22.15
Failure mode	Failure behind/spine	crushing and bending	crushing
h_i [m]	0.8	0.6	0.75
h_k [m]	NA, h_s ca. 1.0	6.6	9*
F_{MaxR}[MN]	89	8.3	3.0
Ice drift [m/s]	0.10	0.00	0.18
Drift direction [°]			23
Maximum level ice event	Molikpaq (Timco and Johnston, 2004)	Confederation Bridge (Brown et al., 2009)	Nordströmgrund (STRICE data, Frederking (2005))
Date/time [dd.mm.yyyy/hr.min]	NA	04.04.2003/07.02	30.03.2003/12.27
Failure mode	NA	crushing and bending	crushing
Mean h_i [m]	2.0	0.58	0.75
F_E [MN]	131	8.9	3.5
Ice drift [m/s]	0.01	1.31	0.02
Drift direction [°]			0
Ratio $\frac{F_{MaxR}}{F_E}$	0.68	0.93	0.86

*approximate keel depth from EM-data times 3, a relation found by linear regression between ULS and EM (Bjerkås, 2006)

calibrated; tilt could be used to find total global loads regardless of the ice drift direction. He assumed that the foundation and lighthouse stiffness was omni directional and that wind loads were negligible. The data was filtered with a 3sec moving average. In the following an attempt is made to compare this ratio to a ratio for an ice ridge.

Based on the calibration done by Frederking (2005), eight quasi-static ice ridge events from the 2003 STRICE- data were analyzed. The maximal ratio between global panel load and tilt was found for an approximately 5m deep ridge. The ratio was 8.2kN/μradians, this value is lower than the value for level ice, suggesting that the total ridge load is not captured.

The ratio above is based on loads measured at MWL, however the actual load point of action for a ridge depends on the ridge depth. In the following estimate the ridge load is approximated by a linearly distributed load with a resultant force F acting at a water depth of $1/3h_k$ (Figure 3). If the lighthouse is approximately a cantilever beam with varying cross section (see Figure 1 and Figure 3) the tilt is given by the equation of rotation of an elastic cantilever beam with

two cross sections 1 and 2 in Equation 1.

$$\theta = \frac{F[(l_2 + l_1)^2 - l_1^2]}{2EI_2} + \frac{Fl_1^2}{2EI_1} \tag{1}$$

where F is the resultant ice load, $l_2 = 7.5m$ is the length of the bottom foundation, l_1 is the distance from the bottom foundation to the load F ($l_1RI \approx 1/3h_k$, $l_1LI \approx MWL$), E is the elastic modulus of the lighthouse. The second area moment is $I = d^4/64$, where d is the diameter, $d_2 = 23m$ and $d_1 = 7.5m$. Now by changing l_1LI to l_1RI according to Figure 3 tilt from the same load for a 5m deep ridge and level ice is compared.

By applying Equation 1 tilt is reduced by approximately 40% for the ridge compared to level ice, due to the change in point of action and the large bottom foundation. As a result the ratio between global panel load and tilt for a 5m deep quasi static ridge should be approximately 20kN/μradians. This estimate needs validation by more advanced numerical tools. Further this analysis shows that it is not possible to find a unique ratio between global load and tilt for ridges.

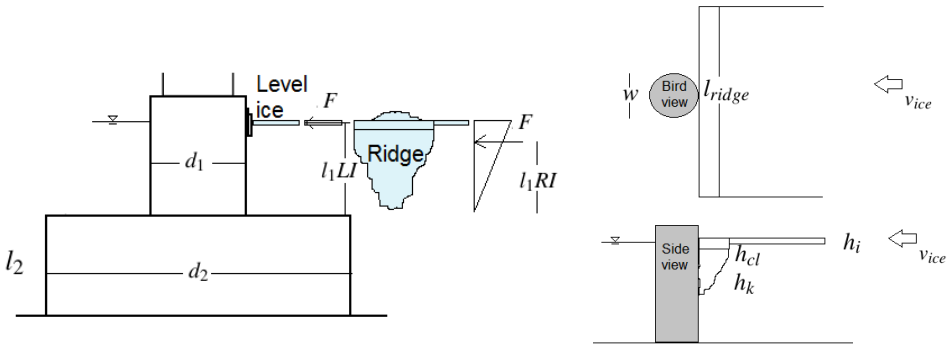

Figure 3. To the left; Simplified level ice and ridge interaction with Nordströmgrund lighthouse. To the right; a ridge interaction seen from above and the side. To illustrate ridge limit ridge building force.

Limit force estimate of critical ridge length

Limit stress is typically applied to estimate dimensioning extreme quasi-static ice loads. In the following a limit stress analysis is applied to estimate minimum ice ridge lengths for crushing to occur on the three structures review in the beginning of this paper. Limit stress requires that the global load from an ice ridge acting on a structure, is lower than the global ridge building force action on the parent ice sheet, illustrated in Figure 3. This is expressed in Equation 2 and 3. It is assumed that the driving forces from the drag and wind are small compared to the ridge building force (Croasdale, 2009).

$$F_i > F_{cl} + F_k + F_s \tag{2}$$

F_i is the ridge building force, F_{cl} is the force from the consolidated layer, F_k is the keel load and F_s is the sail load. Sail loads are assumed to be negligible and are left out of this analysis, this gives Equation 3

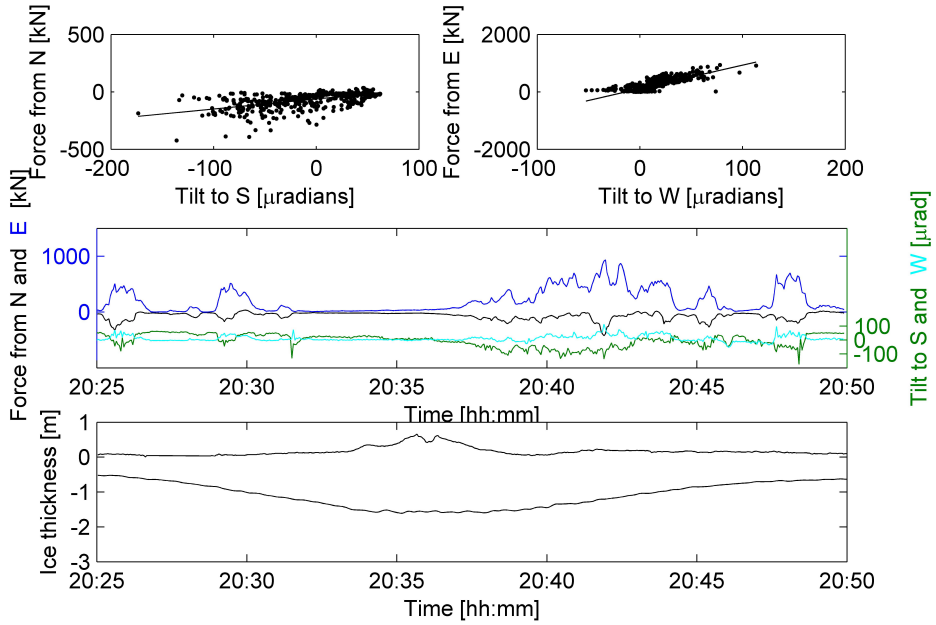

Figure 4. Tilt vs force on the 19th of March 2002 from an ice ridge event, thickness was measured with EM. N (North), S (South), E (East) and W (West).

$$p_i l_{ridge} > p_{cl} w h_{cl} + p_k w h_k \tag{3}$$

p_i is the ridge building force per unit ridge length, l_{ridge} is the length of the ridge, p_{cl} is the ice crushing pressure of the consolidated layer, w is the structure width, h_{cl} is the consolidated layer thickness, p_k is the pressure from the ridge keel and h_k is the keel depth. Ice crushing occur when the ridge length is above a critical length given by Equation 4.

$$l_{ridge} > \frac{p_{cl} h_{cl}}{p_i} w + \frac{p_k h_k}{p_i} w \tag{4}$$

In ISO19906 (2010) the crushing pressure of consolidated layer p_{cl} is given according to Equation 5.

$$p_{cl} = C_R \left(\frac{h_{cl}}{h_{ref}} \right)^n \left(\frac{w}{h_{cl}} \right)^m \tag{5}$$

C_R is a reference strength depending on the area (Beaufort Sea $C_R = 2.8$, Temperature areas $C_R = 1.8$), m is a constant, n is a constant depending on the ice thickness and h_{ref} is 1m. I believe m is a constant used to describe non simultaneous failure over the consolidated layer similar to the Equation ($p_{cl} = A_k D^m h^n$) by Bjerkås (2004), he suggests $-0.3 < m < -0.1$ in ISO19906 (2010) $m = -0.16$.

The reference crushing strength (C_R) in ISO19906 (2010) is 2.8MPa for the Beaufort sea. This value was based on first year and old ice data (ISO19906, 2010). Timco and Johnston (2004) measured ice pressured from first year ice on structures in the Beaufort sea and found that "the maximum Global Pressure measured for all types of ice loading events never exceeded 2 MN/m^2". Based on this; I have changed C_R to 2 for the estimation of critical first year ice ridge length in the Beaufort Sea (Table 5).

In ISO19906 (2010) the rubble keel pressure (Equation 6) is estimated by a passive failure Mohr Coulomb model based on Dolgopolov et al. (1975). In the model the rubble fails simultaneously on shear plans inside the rubble. The original model of (Dolgopolov et al., 1975) was based on observations from model scale tests on ice rubble and the last group in Equation 6 was replaced by $1+2h_k/3w$. The rubble keel pressure p_k is given by Equation 6.

$$p_k = \mu\left(\frac{h_k\gamma_e\mu}{2}+2c\right)\left(1+\frac{h_k}{6w}\right) \tag{6}$$

$$\mu = tan\left(45+\frac{\phi}{2}\right) \tag{7}$$

$$\gamma_e = (1-\eta)(\rho_w-\rho_i)g \tag{8}$$

where μ is the passive pressure coefficient, ϕ is the internal angle of friction at failure, c is the average keel cohesion, w is the structure width and γ_e is the effective buoyancy. Typical values for these ridge parameters are presented in Table 4 based on ISO19906 (2010).

For conical structures a load reduction due to bending failure is expected. ISO19906 (2010) only consider bending of level ice, in the absence of such formulas crushing is considered also for the conical piers of the Confederation bridge.

The ridge building force per unit ridge length is expressed by Equation 9 which is an empirical formula from ISO19906 (2010). The value of R depends on the ice thickness, in ISO19906 (2010) the expression for $Rh_i^{1.25}$ is equal 2, obtained by curve fitting data of 1m thick ice for structure widths greater than 100m. I have used $2 = A = Rh_i^{1.25}$, Equation 9.

$$p_i = Rh_i^{1.25}l_{ridge}^{-0.54} = Al_{ridge}^{-0.54} \tag{9}$$

Finally; the critical ridge length for limit stress is estimated by Equation 10 and presented in Table 5. Ridge parameters are taken from Table 3 and 4. For Nordströmgrund parameters were based on the ridge that caused the largest quasi-static load of 1.3MN. h_{cl} was never measured and is therefor estimated by $h_{cl} = 1.8h_i$ based on measurements by Høyland (2000). For Molikpaq h_k was neither measured, it is estimated by $h_k = 4.5h_s$ based on Timco et al. (2000).

Table 4. Ice ridge parameters used in this estimation (ISO19906, 2010).

Parameter ϕ [°]	c [kPa]	ρ_w [kg/m^3]	ρ_i [kg/m^3]	η [-]
30	7	1025	920	0.3

$$l_{ridge}^{0.46} > \left(p_{cl} h_{cl} + p_k h_k \right) \frac{w}{A} \tag{10}$$

The ridge loads calculated from the analytical models in Table 5 are between 1.5 and 6 times the measured loads.

Table 5. Table over critical length l_{ridge} together with ridge loads F_{cl}, F_k and $F_{tot} = F_{cl} + F_k$. Ridge sizes are taken from Table 3. h_{cl} was not measured for any of the structues and for Molikpaq h_k was also not measured, these values are estimated.

	Molikpaq	Confederation Bridge	Nordströmgrund lighthouse
w [m]	90	14.3	7.6
h_i [m]	0.8	0.6	0.3
h_{cl} [m]	1.44	1.08	0.54
h_k [m]	4.5	6.6	6.1
n	-0.34	-0.38	-0.44
C_R MPa	2*	1.8	1.8
F_{cl} [MN]	118	18	6
F_k [MN]	12	3	2
F_{tot} [MN]	130	21	8
l_{ridge} [m]	9000	200	20

*Adjusted down to 2 from 2.8 to only account for first year ice ridges.

CONCLUSIONS

In this paper actions from first year ice ridges on fixed structures has been studied. The first part of this paper was a review on full scale global loads and associated failure modes on three fixed structures, actions from first year ridges and level ice were compared. The three instrumented structures was the Molikpaq, the piers of the Confederation Bridge and Nordströmgrund lighthouse. In the second part of this paper some ice ridge structure interaction data were analyzed. Data from Nordströmgrund lighthouse were used to obtain a ratio between global panel loads and tilt for ridges compared to level ice. Finally a limit force analysis was performed to estimate minimum ice ridge lengths for crushing to occur on the three fixed structures.

From this work the following conclusions were made:

- The highest ridge loads on Nordströmgrund lighthouse and the piers of the confederation bridge were associated with crushing and combined crushing/bending respectively, while

on Molikpaq crushing of ice ridges did not occur. Measured full scale global ice ridge loads were in the same order as loads from level ice for all three structures.

- From a limit force analysis it was estimated that the critical ridge length to produce local crushing was 9km on Molikpaq compared to 20m for Nordströmgrund lighthouse and 200m on the piers of the confederation bridge.
- From full scale data of a quasi-static 5m deep ice ridge iteration with the Nordströmgrund lighthouse; a ratio between global panel load and tilt was found. The ridge ratio obtained was 8.2 kN/μradians compared to 12kN/μradians for level ice derived by Frederking (2005). The low value indicates that load panels underestimate ridge loads. Additionally; an analytical estimate suggest that the same load from a 5m deep ridge would give approximately 40% less tilt than level ice due to the change of point of action and large bottom foundation. As a result a general ratio between global load and tilt cannot be obtain for ice ridges. For ice ridges; advanced numerical tools (FEM,DEM) are needed to obtain global loads from tilt.

ACKNOWLEDGMENTS

The author wishes to acknowledge the support of the Research Council of Norway through the Centre for Research-based Innovation SAMCoT, and the support of all SAMCoT partners. The author also acknowledges professor Knut V. Høyland for valuable discussions.

REFERENCES

Ahlenius (2005). Arctic map, political, http://www.grida.no/. 2005.

Bjerkås (2004). Global design ice loads' dependence of failure mode. *International Journal of Offshore and Polar Engineering*, (Vol. 3 No. 3).

Bjerkås (2006). Ice actions on offshore structures, with applications of continuous wavelet transform on ice load signals. *Doctoral thesis for the degree of philopophiae doctor, NTNU*.

Bjerkås and Bonnemaire (2004). Ice ridge-structure interaction, Part II: Loads from ice ridges and their surronding ice sheets. *Proceedings of the 17th International Sumposium on Ice*. pp122-129.

Bjerkås, Meese, and Alsos (2013). Ice induced vibrations - observations of a full scale lock-in event. *Proceedings 23rd International Offshore and Polar Engineering Anchorage*. pp1272-1279.

Bonnemaire and Bjerkås (2004). Ice ridge-structure interaction, Part I: Geometry and failure modes of ice ridges. *Proceedings of the 17th International Sumposium on Ice*. pp114-122.

Brown (2001). Four years of ice force observations on the Confederation Bridge. *Proceedings of the 16th International Conference on Port and Ocean engineering under Arctic Conditions (POAC)*. pp285-299.

Brown (2006). Confederation bridge - an innovative approach to ice force. *Proceedings of the 2006 Annual Conference of the Transportation Association of Canada*.

Brown (2007). Analysis of ice event loads derived from structural response. *Cold Regions Science and Technology*, (47). pp224-232.

Brown, Tibbo, Tripathi, Obert, and Shrestha (2009). Extreme ice load events on the Confederation Bridge. *Cold Regions Science and Technology*. 14p.

Croasdale (2009). Limit force ice loads-an update. *Proceedings of the 20th International Conference on Port and Ocean engineering under Arctic Conditions (POAC)*, (30).

Dolgopolov, Afanasiev, Korenkov, and Panfilov (1975). Effect of hummocked ice on piers of marine hydraulic structures. *Third International Symposium on Ice Problems, IAHR*, (Vol. 3 No. 3).

Frederking (2005). Tiltmeter application at Nordströmgrund lighthouse - STRICE project. *Proceedings of the 18th international conference on Port and Ocean engineering under Arctic Conditions*, (Vol 1). pp399-408.

Høyland (2000). Consolidation of first-year sea ice ridges. *Journal of geophysical research*, (Vol. 107, NO C6, 3062).

ISO19906 (2010). Petroleum and natural gas industries - arctic offshore structures. 412p.

Kärna and Jochmann (2004). Field observations on ice failure modes. *Proceedings of the 17th International Symposium on Ice*.

Schwarz and Jochmann (2001). Four years of ice force observations on the Confederation Bridge. *Proceedings of the 16th International Conference on Port and Ocean engineering under Arctic Conditions (POAC)*. pp669-683.

Tibbo, Obert, Shrestha, Tripathi, Mayne, and Brown (2009). Year twelve of the Confederation Bridge ice monitoring program. *Procceedings of the 20th International Conference on Port and Ocean engineering in Arctic Conditions (POAC)*. pp47-57.

Timco and Croasdale (2006). How well can we predict ice loads? *Proceedings of the 18th IAHR International Symposium on Ice*. pp167-174.

Timco, Croasdale, and Wright (2000). An overview of first-year sea ice ridges. *Canadian Hydraulic Centre - technical report*, (5-112). p157.

Timco and Johnston (2004). Ice loads on the caisson structures in the Canadian Beaufort Sea. *Cold regions science and technology*, (No 38). pp185-209.

Timco, Johnston, and Wright (2005). Multi-year ice loads on the Molikpaq: May 12,1986 event. *Proceedings of the 18th International Conference on Port and Ocean engineering under Arctic Conditions (POAC)*, (pp453-462).

Timco, Wright, Johnston, and Frederking (1999). First-year ice ridge loads on Molikpaq. *Proceedings of the 4th International Conference on Development of the Russian Arctic Offshore*. pp172-179.

WMO (1970). WMO sea ice nomenclature. *World Meteorological Organization*, (Tech rep NO 259.TP.145). pp1272-1279.

Wright (1986). Winter ice interactions with an arctic offshore structure. *IAHR International Symposium on Ice Problems 1986*, (Vol. 3 pp49-73).

POAC'15
Trondheim, Norway

Proceedings of the 23rd International Conference on
Port and Ocean Engineering under Arctic Conditions
June 14-18, 2015
Trondheim, Norway

Direct observations of Arctic sea ice thickness variability on seasonal to decadal time scales

Edmond Hansen [1, 2], Sebastian Gerland [2], and Gunnar Spreen [2]
[1]Multiconsult, Tromsø, Norway
[2] Norwegian Polar Institute, Tromsø, Norway

ABSTRACT
Variability in ice thickness observed by moored sonars in the Transpolar Drift in Fram Strait during 1990-2011 is described and quantified. Over the 22 year long period the modal ice thickness decreased by 20% per decade, relative to its long-term average. The mean ice thickness remained relatively constant during 1990-2005, after which it dropped from its prevailing level around 3 m down to 2 m. There are indications of a 6-8 year cycle in modal ice thickness. The cycle's crest to trough difference in thickness is 0.73 m. The cycle is less pronounced in the mean ice thickness, which hints towards thermodynamically controlled processes in explaining the origin of the cycle. The peak-to–peak amplitude of the modal ice thickness seasonal cycle is 0.54 m. The corresponding peak-to-peak amplitude for the mean ice thickness is 1.14 m. The seasonal maximum modal ice thickness in April occurs two months before the corresponding maximum in mean ice thickness in June. The seasonal minimum modal ice thickness in August occurs one month before the minimum in mean ice thickness in September. Combined, this illustrates how different processes control the modal (thermodynamics) and mean (dynamics + thermodynamics/ocean heat) ice thickness.

INTRODUCTION
Arctic sea ice has seen widespread change over the past decades (Meier et al., 2014). A younger and thinner Arctic sea ice cover (Maslanik et al., 2011; Kwok and Rothrock, 2009) remains preconditioned for recent record low sea ice extent minima, such as those in 2007 and 2012 (Parkinson and Comiso, 2013).

It is not straightforward to establish a link between the observed thinning and the drivers of this process. The spatial and temporal resolution of Arctic sea ice thickness data sets available to document long term thinning does not allow a detailed dissection of the ice thickness distribution to be carried out. Often the mean ice thickness is the only summary statistic at hand to document thickness change. The ice thickness distribution is typically bimodal and heavy-tailed, a reflection of how different processes operate differently in different segments over the range of ice thicknesses and ice types. With only the mean ice thickness available to document thinning, it is difficult to conclude on which ice type has changed, and why. Moreover, such long term data sets fail to resolve the seasonal cycle. This complicates the quantification of long term variability.

Here we present time series (1990-2011) of monthly ice thickness distributions obtained by moored sonars in the Transpolar Drift in Fram Strait (Hansen et al., 2013). The spatial and temporal resolution of the data allows us to 1) resolve the full thickness distribution, and 2) resolve the seasonal variability. Here we separate between variability in the thickness of old

level ice and that of the rest of the ice. The variability is quantified for the modal (old ice) and mean ice thickness as deduced from the monthly ice thickness distributions.

The Fram Strait data set was presented by Hansen et al. (2013). The present contribution takes this previous study one step further by identifying and quantifying variability on three time scales; seasonal, interannual and decadal or longer.

DATA AND METHODS

The data set comprises 22 years (1990-2011) of continuous draft observations by moored upward looking sonars in the Transpolar Drift at 79° N 5° W in Fram Strait (Figure 1, and Hansen et al. 2013). During 1990-2006 the observations were made with CMR ES300 sonars operating with a sampling rate of 4 min. The instrumentation was replaced by ASL IPS sonars in 2006, operating with a sampling rate of 2 s. Installed at a depth of 50 m, the nominal footprint of the sonars is approximately 1.8 m. The full data set was processed and quality controlled by ASL Environmental Sciences following the methodology of Melling et al. (1995). Further details about the data set and its processing are found in Hansen et al. (2013).

The draft values were converted to ice thickness by multiplying with the factor 1.136 (empirically derived by Vinje and Finnekåsa, 1986). This simplified conversion is only made to facilitate a direct comparison with ice thickness data sets. The conversion is linear, the original draft value may be obtained by dividing with this factor. Monthly normalized ice thickness distributions were constructed by binning, counting, and normalizing the thickness observations month by month. The accuracy of summary statistics like the modal and mean ice thickness is within the bin width of the monthly thickness distributions of 10 cm (Vinje et al. 1998; Hansen et al. 2013).

The thickness series used to construct the monthly ice thickness distributions are time referenced (the quality of concurrent ice drift velocity observations is too poor to carry out a conversion to spatially referenced thickness series). In practice this means that the sampling distance is varying with time, and that the statistics derived for each month are based on segments of ice of different distances. However, subsampling with different subsampling periods shows little effect on the monthly statistics (Hansen et al., 2013). Statistical modelling of the effect of time varying ice drift demonstrates the same insensitivity in the monthly summary statistics to the drift (Uteng et al., in prep.).

The observation site in Fram Strait is illustrated in Figure 1. The figure also shows the backward trajectories of ice exported through Fram Strait for each month of the observation period (Hansen et al., 2013). This illustrates the source regions of the ice observed in Fram Strait. In investigating variability in this dynamic region, it is imperative that variability due to advection is separated from that of any other causes. Hansen et al. (2013) found little relation between thickness variability and advection patterns on any time scale.

The objective of this study is to identify and quantify variability in ice thickness over the timescales seasonal, interannual and decadal or longer. The term seasonal variability is used to address the variability over each year (the seasonal cycle). Interannual variability is referring to variability in thickness on timescales 1-9 years. When using the term decadal or longer variability we are referring to variability with periods over scales longer than 10 years.

The seasonal variability of the thickness of sea ice drifting through Fram Strait is quantified by averaging the modal and mean ice thickness over all available calendar months into an

average seasonal cycle. Due to the longer scale variability, the cycle is calculated around the average modal and mean ice thickness for each year, respectively. The interannual variability is highlighted by filtering out the seasonal cycle. The filter is a three-step centred simple moving average with a window of 13 months in the first step, then 9 and 7 in the two subsequent steps. The time series contains individual months with missing data. A total of 52 months are missing in the 252 months long time series. In order to enable the filtering to be performed, the gaps were filled by using the average value of the same month the preceding and succeeding year to fill the gap for each missing month. This approach ensures that any cyclicity in the time series is maintained.

We apply two other methods of smoothing to ensure that the gap filling technique does not introduce artefacts: First we reproduce the annual averages presented by Hansen et al. (2013), where years with missing months were represented by the average of the remaining months. Secondly, we do the smoothing on the segments of data between the missing months with a centred simple moving average with a 13 month window. The combination of these two methods supplements the method of filling the gaps.

Finally an indication of long term variability (or change) is indicated by a linear fit through the data points. The fit start in August 1990, and ends in August 2011. In a time series featuring cyclicity, such a fit is sensitive to the location of the start and end points. Ideally any cyclicity should be removed from the time series prior to the fit. However, our time series is not long enough to precisely identify the period of any cyclicity on longer time scales. The fit is therefore crudely made across the entire time series, as an indication of the variability or change over the entire 22 years long observation period.

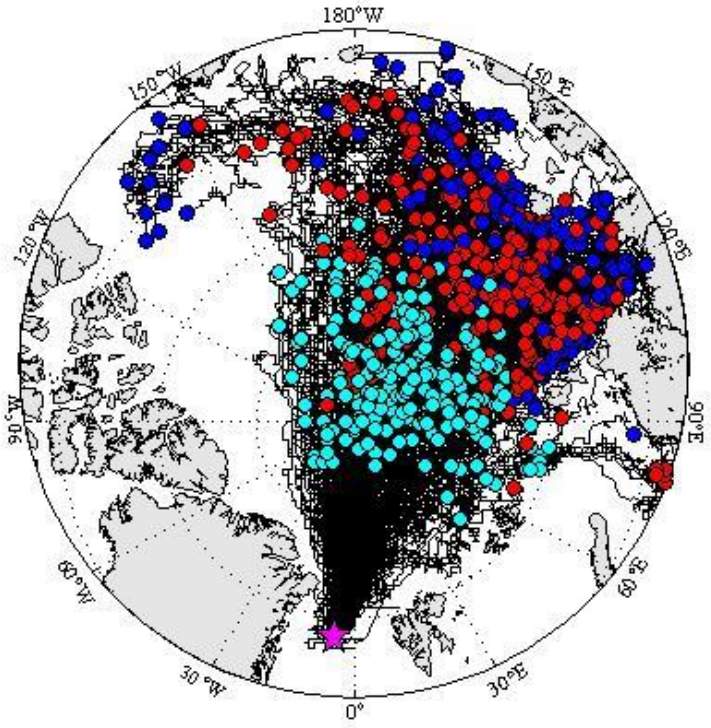

Figure 1. The location of the observation site in Fram Strait (magenta star). The black lines show the ice trajectories, calculated backward from the observation site from the month of observation up to 3 years earlier. The bullets indicate the position of the ice 1 (cyan), 2 (red) and 3 (blue) years prior to the observation of its thickness in Fram Strait (adapted from Hansen et al., 2013).

RESULTS

Long term trend: Variability on decadal or longer time scales

The time series of modal ice thickness is presented in Figure 2. It is too short to provide detailed information about the different modes of variability in the Arctic occurring om time scales from decadal and longer (e.g., Venegas and Mysak, 2000; Hilmer and Lemke, 2000; Polyakov and Johnson, 2000). However, even a trend derived from a plain linear regression may provide information about the scale of variability or change over the observation period. For that purpose we use the time series where the occasional gaps in monthly values are filled.

The linear trend of the modal ice thickness, bluntly taken across seasonal and interannual variability, is estimated to be negative at -0.51 m per decade (Figure 2 a). This corresponds to -20% per decade, relative to the long term average modal thickness.

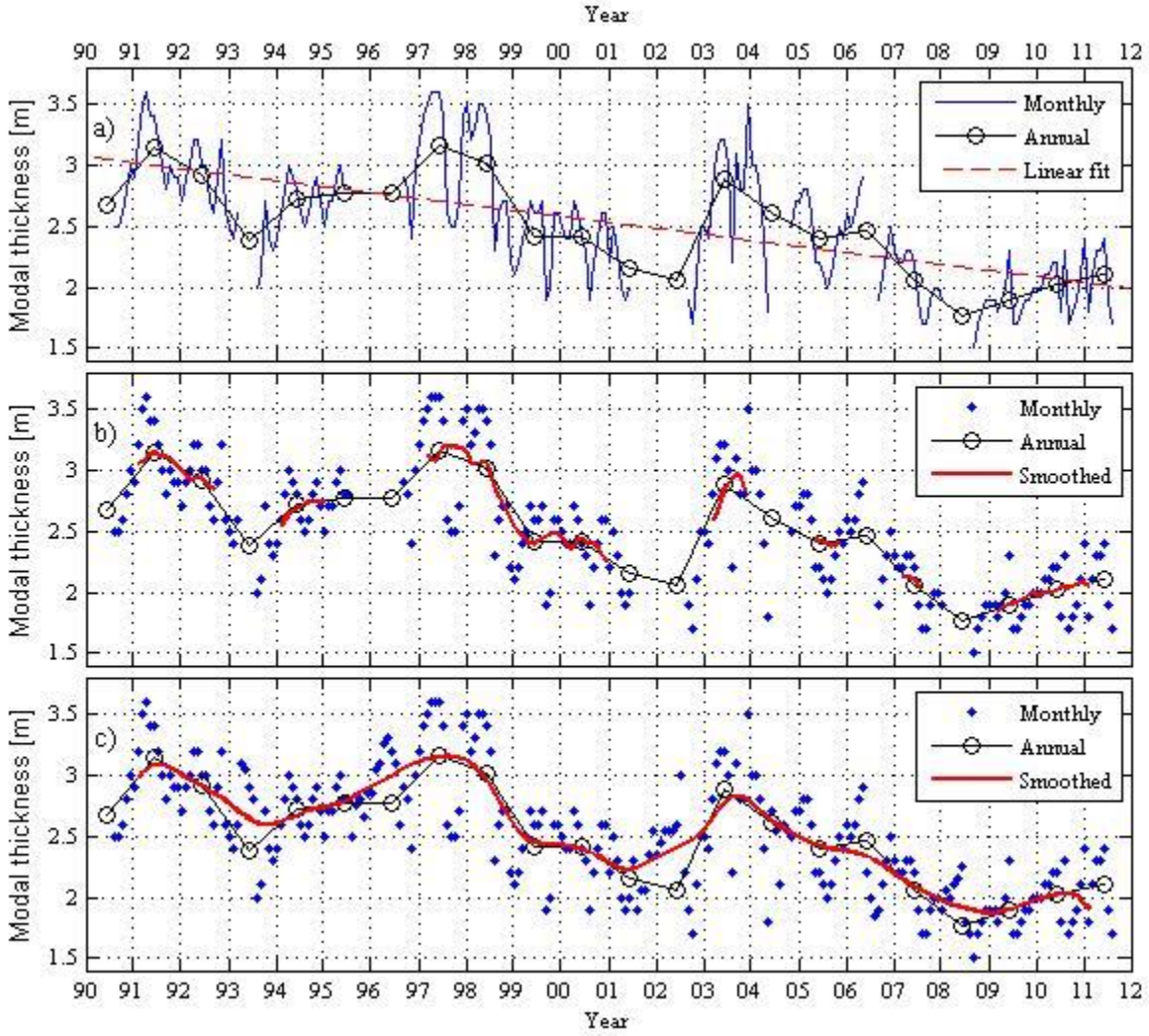

Figure 2. Time series of modal (old ice) thickness observed in Fram Strait during 1990-2011. To ensure readability the same data is presented over three panels, highlighting different approaches to address the variability. The upper panel (a) shows the monthly and annually averaged data, along with a linear fit to the monthly data. The middle panel (b) shows the monthly values, along with a smoothed version (13 month simple centred running average) of the data segments between missing data. The lower panel (c) shows the monthly time series with filled gaps. It also shows its smoothed version (triple running mean, centred, 13 month window).

The time series of mean ice thickness is shown in Figure 3. A linear regression analysis across the whole time series yields a negative trend at -0.36 m per decade (Figure 3 a). This corresponds to –12% per decade, relative to the long term average of the mean ice thickness. However, in this case the linear model appears less representative for the change over the 22 year long period. Considering the smoothed curves in Figure 3 b) and c) where the seasonal variability is filtered out, the mean ice thickness appears to remain around 3 m from 1990 to 2006. It then plummets down to approximately 2 m over only 4-5 years.

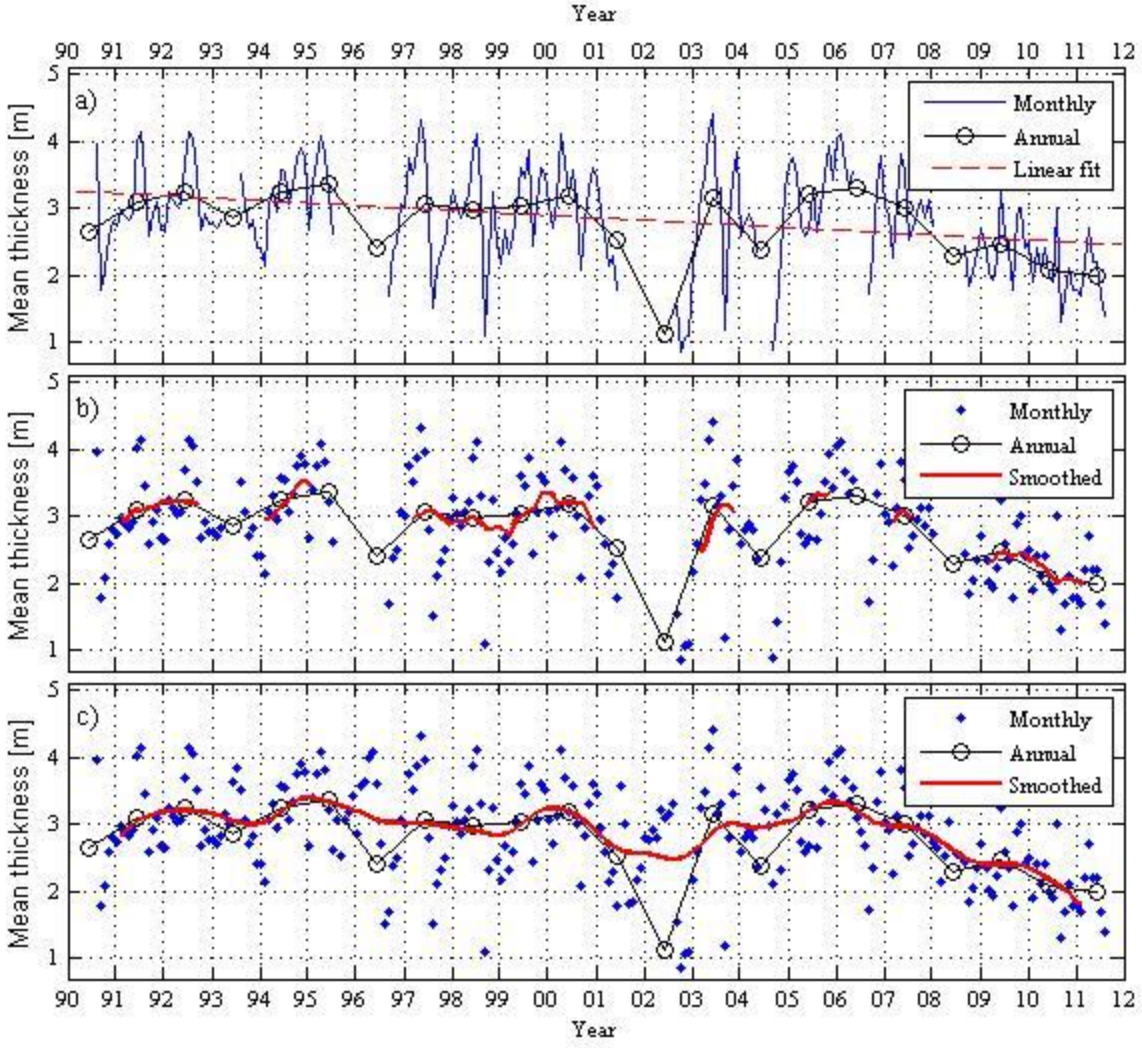

Figure 3. Time series of mean ice thickness observed in Fram Strait during 1990-2011. The content of panels a), b) and c) follows the structure as outlined in the caption of Figure 2.

Interannual variability

The seasonal cycle of the modal ice thickness should be filtered out to highlight variability on timescales longer than seasonal. Due to occasional gaps in the time series, we must either do the filtering on the data segments between the gaps, or fill the gaps. The first approach may result in loss of information, while the latter may introduce artefacts. Here we have done both, in addition to adding the annual averages of Hansen et al. (2013) (where the average of years with missing months were represented by the average of the remaining months). This reduces the risk of misinterpretation of the smoothed curves.

The result for the modal thickness is presented in Figure 2 b) and c). The two versions of the smoothed curves are seen to behave in a similar pattern. The annual averages are also seen to follow the smoothed curves, except for the years containing data gaps where there are deviations. Based on the three approaches combined, we conclude that superimposed on the downward trend there is interannual thickness variability on time scales of 6-8 years. The apparent crests at the start and end of the times series in 1991 and 2010/11 is excluded from these considerations, due to the risk of artefacts from the smoothing process. Crests in 1997 and 2003, combined with troughs in 1993, 2001 and 2008/09, nevertheless indicate the potential existence of a periodic cycle.

For the purpose of identifying the amplitude of this apparently periodic cycle in modal thickness, we detrend the curve of monthly modal ice thicknesses by subtracting the linear fit. The result is seen in Figure 4. Counting from the start in 1990, there are three troughs. Their amplitudes are -0.30 m, -0.29 m and -0.25 m. Correspondingly there are two crests, with amplitudes 0.45 m and 0.44 m. This provides four peak-to-peak amplitudes; 0.75 m (1993-1997), 0.74 m (1997-2001), 0.73 m (2001-2003) and 0.70 m (2003-2008).

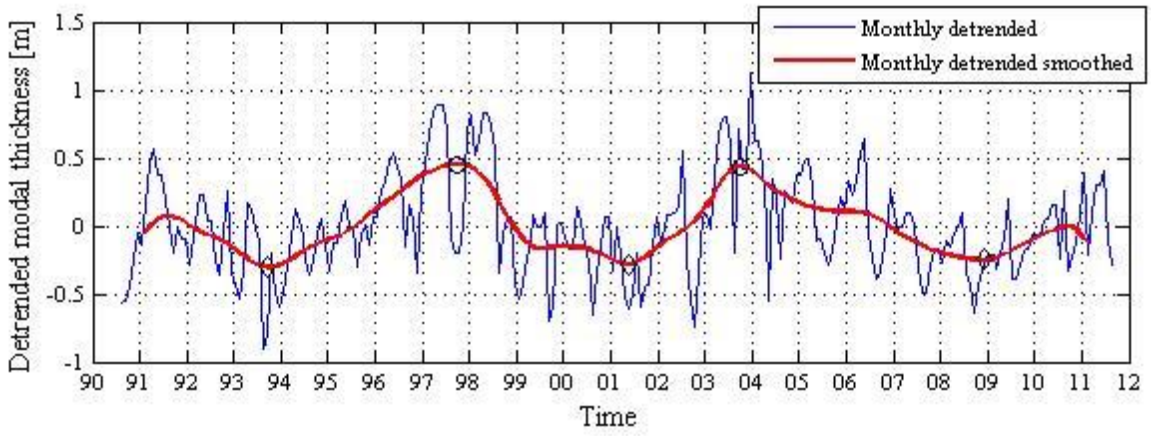

Figure 4. The detrended modal ice thickness from Fram Strait. The detrending is carried out on the monthly time series with filled gaps, by subtracting the linear fit from the monthly values. The time series is smoothed to highlight interannual and decadal variability. Troughs are indicated with a diamond, while crests are indicated by a circle.

Figure 3 b) and c) shows the smoothed mean ice thickness. There are indications of variability on the same 6-8 year time scale time as for the modal thickness, but for the mean ice thickness this is much less pronounced. There is variability though, with the smoothed mean ice thickness varying from 3.2 m to 2.5 m over just 2-3 years (2000-2003). The most pronounced feature of variability (or change) is the drop in mean ice thickness starting in 2006 (from 3.2 to 2 m over 5 years).

Seasonal variability

The average seasonal cycle in modal thickness (the thickness of old level ice) over the 1990-2011 period is shown in Figure 5. On average, the maximum thickness is reached in April, when the ice is 0.23 m thicker than the annual average. The minimum modal thickness is reached in August; the ice is then -0.31 m thinner than the annually averaged thickness. This yields a seasonal peak-to-peak amplitude of 0.54 m around the average thickness over the year. This is the work of thermodynamical processes during freeze and melt. Clearly the magnitude of thickness gain or loss during the seasons varies with the factors controlling the

seasonal freezing and melting. In addition to the thermodynamic factors, the age of the ice is a major factor in controlling the level of the thickness which the seasonality cycles around. Hence advection also plays a role in the sense that ice that is not exported to lower latitudes may survive the melt season to form older ice. The average seasonal cycle observed in Figure *5* is reflecting the work of the average thermodynamic factors and the prevailing age of the ice during this period.

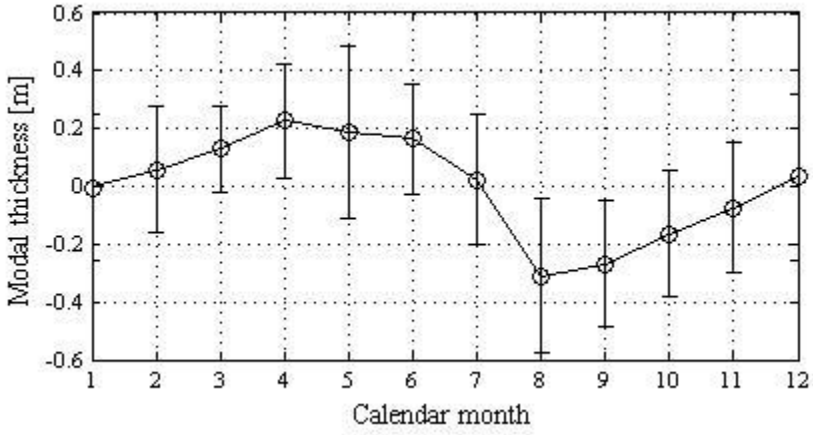

Figure 5. The average seasonal cycle of the modal ice thickness observed in Fram Strait during the period 1990-2011. The error bars show the standard deviation of each monthly average.

The average seasonal cycle of the mean ice thickness in Fram Strait over the 1990-2011 period is shown in Figure 6. The monthly mean ice thickness is calculated as the arithmetic mean of all thickness observations during each month since the onset of the observations in 1990. Unlike the modal thickness, which is reflecting the thickness of old level ice and where the variability reflects variability in thermodynamic processes, the mean ice thickness is influenced by all available ice types. Moreover, variability in the mean ice thickness generally reflects variability in both thermodynamic and dynamic processes acting on the ice to change its thickness. Clearly the mean ice thickness it is not a summary statistic which is well suited to describe ice thickness change or to point to likely causes for the change. However, it is much used to describe the thickness of the ice cover in reports from large scale ice models or large scale ice thickness observations, or in reports based on ice thickness data sets where the temporal and spatial coverage does not allow more details than the mean thickness to be deduced.

During 1990-2011 the maximum seasonal mean ice thickness is reached in June, when it peaks to 0.43 m above the annual average. The seasonal minimum is reached in September at -0.70 m. The average seasonal peak-to-peak amplitude of the mean ice thickness is therefore 1.14 m around the annually averaged mean thickness. In addition to the thermodynamic processes and ice age which controls the thickness of level ice, the mean ice thickness is also controlled by dynamic processes (rafting, ridging and rubble building). The mean ice thickness is dominated by dynamically deformed ice, due to the generally great thicknesses of this ice type. On average 66% of the mean ice thickness is due to deformed ice in this region (Hansen et al., 2014). However, it is not straightforward to separate between the role of dynamic and thermodynamic processes in controlling the seasonal thickness change.

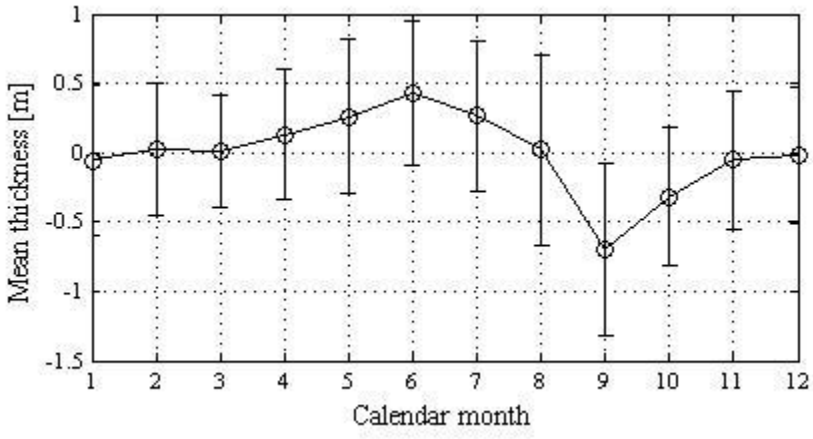

Figure 6. The average seasonal cycle of the mean ice thickness in Fram Strait during the period 1990-2011. The error bars show the standard deviation of each monthly average.

DISCUSSION

The variability in modal and mean ice thickness is observed to behave differently on all timescales. This illustrates how the physics controlling the modal and mean ice thickness differ. The first parameter is largely controlled by thermodynamic processes. The latter is dominated by ridged ice (Hansen et al., 2014), hence dynamic processes are dominating in increasing the value of this parameter. On the other hand thermodynamics play a major role in taking the mean ice thickness down, since ridged ice is particularly vulnerable to ocean heat (Amundrud et al., 2006). Since the sensitivity to ocean heat is much larger for ridged ice than for level ice, the difference in variability between modal and mean ice thickness should be expected.

In the seasonal cycle the difference in controlling processes is reflected in the timing of seasonal maxima and minima. The seasonal maximum in modal ice thickness is reached in April, the last month where freezing dominates the freeze/melt balance. For the mean ice thickness the seasonal maximum is reached two months later in June. A possible explanation is that the ridging process continues to operate on the surviving thin ice until this month, even after surface melt has started to occur. Correspondingly the seasonal minimum in modal thickness is reached in August, one month prior to the minimum in mean ice thickness. A likely contributing factor, is that ocean heat accumulated during summer is available to melt and disintegrate the deep and porous ridges, while the less ocean heat sensitive level ice floats in a fresher and more rapidly cooling surface layer.

The difference in timing of seasonal maximum and minimum is also likely to be affected by the fact that melt/freeze may change the modal and mean ice thickness in different directions. At onset of melt during spring, thin ice and old level ice becomes thinner. The modal thickness is decreasing. However, the removal of thin ice from the distribution acts to increase the mean ice thickness of the surviving ice. (Statistically speaking, the false conclusion that melting ice becomes thicker is an example of the effect of a survivorship bias. It is, therefore, also an example of how one should be careful when using the mean ice thickness to interpret the effect of processes in play). Likewise, at the onset of freeze during fall, new and thin ice is added while the modal thickness is increasing. However, the addition of thin ice in the distribution may act to reduce the mean ice thickness.

The drop in mean ice thickness from 3 m to 2 m during 2006-2011 is not reflected in the modal ice thickness in the same way. This decrease in mean ice thickness occurred during a period where both the number and average depth of ridges decreased (Ekeberg et al., 2014). The reason for this loss of ridged ice in the Transpolar Drift in Fram Strait remains unresolved; it might be connected to changes in both ridge formation and/or ridge degradation processes. However, the fact that this loss of ridged ice occurred concurrent with a shift towards younger ice (Hansen et al. 2013; Maslanik et al., 2011) points to a contributing factor: Younger ice contains larger fractions of young ridges, which are more prone to disintegration than their older consolidated counterparts. When facing increased ocean heat storage in the upper ocean (Stroeve et al., 2014) it is expected that such young ridges are effectively eroded, thereby taking the mean ice thickness drastically down.

The apparent 6-8 year cycle in modal thickness is intriguing. Comiso (2012) saw indications of an 8-9 year cycle in his time series (1978-2010) of area covered by multiyear ice. Such variability in age composition is likely to affect the modal thickness. Another possible source of the cycle is thickness anomalies formed in the Siberian shelf seas and in the Chukchi Sea, which propagate across the Arctic Ocean to Fram Strait and contribute to thickness anomalies with timescales of about 9 years (Koenigk et al., 2006). However, our time series is too short to conclude on the long-term consistency, origin and significance of the cycle observed in the modal ice thickness. It is therefore important to continue the observations of ice thickness in Fram Strait.

CONCLUSIONS

Variability on seasonal, interannual and decadal or longer time scales in monthly values of modal and mean ice thickness observed in the Transpolar Drift in Fram Strait is described. The time series were obtained by moored upward looking sonars during the period 1990-2011.

The peak-to–peak amplitude of the modal ice thickness seasonal cycle is 0.54 m. The corresponding peak-to-peak amplitude for the mean ice thickness is 1.14 m. The seasonal maximum modal ice thickness in April occurs two months before the corresponding maximum in mean ice thickness in June. The seasonal minimum modal ice thickness in August occurs one month before the minimum in mean ice thickness in September. This difference in timing illustrates how different processes control the two parameters.

There are indications of a 6-8 year cycle in modal ice thickness. The cycle's crest to trough difference in thickness is 0.73 m. The cycle is less pronounced in the mean ice thickness, which hints towards thermodynamically controlled processes in explaining the origin of the cycle. However, our time series is too short to conclude on the long-term consistency, origin and significance of the cycle.

Variability (or change) on decadal or longer time scales was quantified by the linear trend through the data. The linear trend of the modal ice thickness was estimated to be negative at -0.51 m per decade. This corresponds to -20% per decade, relative to the long term average modal ice thickness. The linear trend in the mean ice thickness was found to be negative at -0.36 m per decade (12% relative to the long term average mean ice thickness). However, a pronounced decrease from 3.2 m to 2 m over the period 2006-2011 is the most pronounced long term feature of the mean ice thickness time series.

REFERENCES

Amundrud, T. L., H. Melling, R. G Ingram, and S. E. Allen (2006), The effect of structural porosity on the ablation of sea ice ridges, J. Geophys. Res., 111, C06004, doi:10.1029/2005JC002895.

Comiso, J. C. (2012), Large decadal decline in the Arctic multiyear ice cover, J. Clim., 25, 1176-1193, doi: http://dx.doi.org/10.1175/JCLI-D-11-00113.1.

Ekeberg, O-C., K. Høyland, E. Hansen and M. Tschudi (2014), Reduction in the Number and Draft of Ridges in the Transpolar Drift in the Fram Strait during 2006-2011, In Proceedings of the 22nd IAHR International Symposium on Ice, doi:10.3850/978-981-09-0750-1_1226, pp. 574-581.

Hansen, E., S. Gerland, M. A. Granskog, O. Pavlova, A. H. H. Renner, J. Haapala, T. B. Løyning, and M. Tschudi (2013), Thinning of Arctic sea ice observed in Fram Strait: 1990-2011, J. Geophys. Res.,Vol. 118, doi:10.1002/jgrc.20393.

Hansen, E., O-C. Ekeberg, S. Gerland, O. Pavlova, G. Spreen, and M. Tschudi (2014). Variability in categories of Arctic sea ice in Fram Strait. J. Geophys. Res. – Oceans, vol. 119, Issue 10, pp. 7175-7189, doi:10.1002/2014JC010048.

Hilmer, M., and P. Lemke (2000), On the decrease of Arctic sea ice volume, Geophys. Res. Lett., 27(22), 3359-3362,doi:10.1029/2000GL011403.

Koenigk, T., U. Mikolajewicz, H. Haak, and J. Jungclaus (2006), Variability of Fram Strait sea ice export: Causes, impacts and feedbacks in a coupled climate model, Clim. Dyn., 26,17-34, doi:10.1007/s00382-005-0060-1.

Kwok, R., and D. A. Rothrock (2009), Decline in Arctic sea ice thickness from submarine and ICESat records: 1958-2008, Geophys. Res. Lett., 36, L15501, doi:10.1029/2009GL039035.

Maslanik, J. A., J. Stroeve, C. Fowler, and W. Emery (2011), Distribution and trends in Arctic sea ice age through spring 2011, Geophys. Res. Lett., 38, L13502, doi:10.1029/2011GL047735.

Melling, H., P.A. Johnston, and D.A. Riedel (1995), Measurement of the draft and topography of sea ice by moored subsea sonar, Journal of Atmospheric and Oceanic Technology, 13(3), 589-602.

Meier, W. N., and 11 others (2014), Arctic sea ice in transformation: A review of recent observed changes and impacts on biology and human activity, Rev. Geophys., 51, 185-217, doi:10.1002/2013RG000431.

Parkinson, C. L., and J. C. Comiso (2013), On the 2012 record low Arctic sea ice cover: Combined impact of preconditioning and an August storm, Geophys. Res. Lett., 40, 1356-1361, doi:10.1002/grl.50349.

Polyakov, I., and M. Johnson (2000), Arctic decadal and interdecadal variability, Geophys. Res. Lett., 27(24), 4097-4100, doi:10.1029/2000GL011909.

Stroeve, J., T. Markus, L. Boisvert, J. Miller and A. Barret (2014), Changes in Arctic melt season and implications for sea ice loss, Geophys. Res. Lett., 41, 1216-1225, doi:10.1002/2013GL058951.

Venegas, S., and L. Mysak (2000), Is there a dominant timescale of natural climate variability in the Arctic?, J. Clim., 13, 3412-3434, doi: http://dx.doi.org/10.1175/1520-0442(2000)013<3412:ITADTO>2.0.CO;2.

Vinje, T., and Ø . Finnekåsa (1986), The ice transport through Fram Strait, *Norsk Polarinstitutt Skrifter*, No. 186, Norwegian Polar Institute *Skrifter* Series.

Vinje, T., N. Nordlund, and Å. Kvambekk (1998), Monitoring ice thickness in Fram Strait, J. Geophys. Res., Vol. 103, No. C5, pp. 10,437-10,449.

POAC'15
Trondheim, Norway

Proceedings of the 23rd International Conference on
Port and Ocean Engineering under Arctic Conditions
June 14-18, 2015
Trondheim, Norway

SIBIS: A NUMERICAL ENVIRONMENT FOR SIMULATING OFFSHORE OPERATIONS IN DISCONTINUOUS ICE

Ivan Metrikin[1], Arne Gürtner[1]
Basile Bonnemaire[2], Xiang Tan[2], Arnt Fredriksen[2], Dmitry Sapelnikov[2]
[1] Arctic Technology Department, Statoil ASA, Trondheim, Norway
[2] Multiconsult AS, Tromsø, Norway

ABSTRACT
Exploration and production of oil and gas resources in harsh offshore environments may require operating in contact with ice. Therefore, there is a need to understand the operational implications of ice actions on stationkeeping of floating platforms, offloading of hydrocarbons, evacuation and rescue of personnel and oil spill response operations. This knowledge is especially important in the early phase of field developments projects, because ice actions can strongly affect the costs of the hull structure of a floating platform, as well as the design of its mooring and propulsion systems. Furthermore, estimating the operational expenditures of potential support operations requires the knowledge of ice loads on vessels in transit during physical ice management and other special operations such as iceberg towing through broken ice. This paper presents a novel numerical environment for simulating such complex and critical offshore operations with high fidelity and performance: SIBIS, which stands for "**S**imulation of **I**nteraction between **B**roken **I**ce and **S**tructures". The numerical model estimates both local and global ice actions on vessels and offshore structures, and the corresponding structural response in time domain. This paper describes the overall structure and capabilities of the SIBIS package, and presents some examples of its successful usage in industrial projects.

INTRODUCTION
Oil and gas industry operations in deep-water Arctic areas are currently taking place primarily during the open water season. For example, floating drilling and production platforms are routinely operating in the Barents Sea and offshore Newfoundland and Labrador. However, certain offshore sites may experience rare sea ice intrusions, and in such situations the performance of a drilling or production facility shall remain safe and robust. It is known that in all practical sea ice intrusion situations the ice cover approaching the operational site of a floating platform will be discontinuous, i.e. broken into discrete ice features of various shapes and sizes either by waves or by the operator's ice management fleet.

The capability of a platform or a vessel to operate in a broken ice field depends on the level of ice actions. These actions, in turn, depend on the ice-structure interaction processes which involve complex contact mechanics: ice material failure, rigid-body motions of the broken ice pieces, ice-ice and ice-structure friction, ice clearing processes and fluid effects. Moreover, the boundary conditions of the broken ice domain may have a strong influence on the load-response relationship of the dynamical ice-structure system, leading to a range of highly nonlinear and complex physical behaviours. Such interactions are very challenging to describe and predict, and the industry lacks reliable engineering tools for computing the response of structures to actions from broken ice.

Modelling and simulation of the global loads on structures from broken ice is especially challenging because of the apparent discrete-continuum nature of the broken ice material. On the one hand, it is composed of distinct ice floes that can be described as separate independent bodies, i.e., a discrete system. On the other hand, during ice drift and ice-vessel interactions the ice floes can crush, split, buckle and fracture, producing new floes and brash ice. Such material behaviour can be difficult to describe from a purely discrete perspective, and calculations of stresses and strains inside the individual ice floes may be necessary. Nevertheless, several empirical and numerical methods have been developed for estimating global loads on offshore structures from broken ice.

State-of-the-art empirical methods can be listed as follows:

- Methods based on regression analyses of model tests performed in pack ice conditions (Spencer and Molyneux, 2009; Woolgar and Colbourne, 2010; Wang et al., 2010);
- The "equivalent level ice thickness" method of Keinonen et al. (1998);
- Formulae derived from full-scale measurements of the global ice loads on the Kulluk platform (Wright, 1999; Croasdale et al., 2009; Palmer and Croasdale, 2013).

However, those empirical formulations produce only one estimate of the ice load for a certain combination of ice-vessel parameters. For practical applications that can be insufficient, especially when reliable information about the dynamical and statistical characteristics of the ice load signal are needed for an engineering application (such as the mean and peak values). Although this limitation can be circumvented by either a statistical method (Metrikin et al., 2013) or a "max-to-mean ratio" method (Eik and Aksnes, 2010; Eik, 2011), such methods do not seem to be widely applied in the industry. Another promising empirical approach is based on direct usage of experimental data of the measured global ice loads, which are used as input to a numerical model of an offshore structure. Although this method has been widely used in dynamic positioning (DP) applications (Jenssen et al., 2009; Hals and Jenssen, 2012; Metrikin et al., 2013), the most challenging stationkeeping scenarios, such as DP position loss due to insufficient thrust, cannot be reliably replicated by this method as demonstrated by Jenssen et al. (2012) and Metrikin et al. (2013).

It is generally accepted that a more promising approach is to utilize a high-fidelity numerical model, based on the fundamental laws of physics, to estimate the ice loads. Different numerical techniques have been historically applied for this purpose:

- The Finite Element Method (FEM) implemented in a commercial software package such as LS-DYNA, ANSYS or ABAQUS (Wang and Derradji-Aouat, 2010; Wang and Derradji-Aouat, 2011; Millan and Wang, 2011; Lobanov, 2011; Kim et al., 2013; Lee et al., 2013; Kim et al., 2014);
- Implementation of the Particle-In-Cell (PIC) method introduced by Sayed (1997) and further developed at the National Research Council of Canada (Barker et al., 2000, 2002, 2014; Barker and Sayed, 2012; Iyerusalimskiy et al., 2012; Sayed and Barker, 2011; Sayed and Kubat, 2011; Sayed et al., 2012a, 2012b, 2014a, 2014b, 2015; Vachon et al., 2012);
- Various implementations and further developments of the classical penalty-based discrete element method of Cundall (1971). Modern implementations include:
    - Finite-Discrete Element Method (FEM-DEM) numerical code developed in-house by the Department of Applied Mechanics at Aalto University in Finland (Tuhkuri, 2005; Paavilainen et al., 2006, 2009, 2011; Paavilainen and Tuhkuri, 2012; 2013; Paavilainen, 2013; Polojärvi and Tuhkuri, 2009, 2010, 2013,

2014; Polojärvi et al., 2012, 2015; Polojärvi, 2013; Haase et al., 2010; Ranta et al., 2014);
    - Model of the Krylov State Research Centre in Saint-Petersburg, Russia (Karulin and Karulina, 2010, 2011, 2013, 2014);
    - The DECICE code owned by the Oceanic Consulting Corporation in Canada (O'Brien, 2004; Quinton, 2006; Lau, 2006; Lau and Ré, 2006; Lawrence, 2009; Liu et al., 2010; Zhan et al., 2010; Park et al., 2011; Lau et al., 2011; Molyneux et al., 2012a, 2012b; Zhan and Molyneux, 2012);
    - And other independent developments (Selvadurai, 2009; Sun and Shen, 2012; Vroegrijk, 2012; Ji et al., 2014, 2013).
- Recently, a new method for calculating broken ice loads on structures was proposed - the GPU-based event mechanics (GEM) (Daley et al., 2012, 2014a, 2014b; Alawneh et al., 2015). The background theory and governing equations of that method can be found in Alawneh (2014), and validation was performed against small-scale experiments where the vessel and the ice floes were modelled by polypropylene blocks (Alawneh, 2014; Alawneh et al., 2015).

In the authors' opinion, one of the most promising numerical approaches for simulating ice-structure interaction is the nonsmooth discrete element method. For ice mechanics applications that method was pioneered by Konno and Mizuki (2006a), and was developed further in their subsequent publications (Konno and Mizuki, 2006b; Konno et al., 2007, 2011, 2013; Konno and Yoshimoto, 2008; Konno, 2009a, 2009b; Konno and Saitoh, 2010; Watanabe and Konno, 2011; Ishibashi et al., 2014). A similar approach is utilized in the numerical model developed by the Ship Modelling and Simulation Centre (SMSC) in Trondheim, Norway (Amdahl et al., 2014; Gürtner et al., 2012; Lubbad and Løset, 2011), and in the simulator product developed by the Norwegian University of Science and Technology (Metrikin et al., 2012a, 2012b, 2013, 2015; Metrikin and Løset, 2013; Kerkeni et al., 2013a, 2013b; Kerkeni and Metrikin, 2013; Scibilia et al., 2014; Østhus, 2014; Metrikin, 2014; Kjerstad and Skjetne, 2014; Kjerstad et al., 2015). Furthermore, the nonsmooth discrete element approach is presumably utilized in the new ice simulation tool using a multi-model program developed by Cervval, Bureau Veritas and Technip (Septseault et al., 2014, 2015). Finally, another numerical model, seemingly based on similar theoretical principles, is currently being developed independently by the Norwegian University of Science and Technology within the framework of the Sustainable Arctic Marine and Coastal Technology (SAMCoT) centre for research-based innovation (Lubbad and Løset, 2015).

This paper presents a novel and independently developed numerical approach for estimating the response of vessels and offshore structures to broken ice actions. The approach is based on the nonsmooth 3D formulation of the discrete element method, and it is implemented in a software package which offers a complete engineering environment for simulating various offshore operations in contact with ice. The forthcoming sections of the paper describe the structure and capabilities of the new software package, as well as some of its validation cases and successful usage examples from real industrial projects.

SIBIS MODEL DESCRIPTION

SIBIS (**S**imulation of **I**nteraction between **B**roken **I**ce and **S**tructures) is a novel simulation tool which has been developed jointly by Statoil and Multiconsult as a complete numerical environment for efficient simulations of offshore structures in discontinuous ice conditions in time domain. The main application of the SIBIS numerical model is simulating the response of floating structures to global pack ice loads, but the software can also be used for simulating

ice actions on fixed offshore and coastal structures in intact or deformed (e.g. ridged) ice, as well as for a wide spectrum of other ice engineering challenges, such as for example under-hull ice material transport investigations. On the highest level the SIBIS numerical tool is structured as shown in Figure 1.

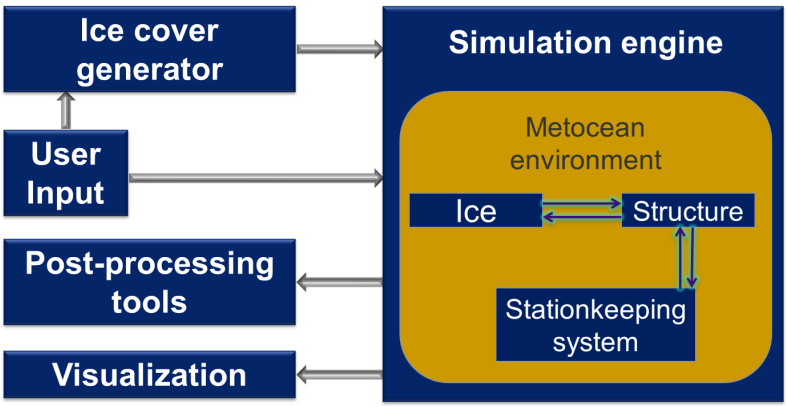

Figure 1. Top-level structure of the SIBIS simulator product.

User's input to the numerical model includes the 3D surface mesh of the simulated structure, its mass and inertia tensor, as well as the stationkeeping system configuration. The structure can be moored or thruster-assisted (on DP), as well as fixed to a planar motion mechanism (PMM) or to a towing carriage in a virtual ice basin. Other user-defined input parameters to SIBIS include the densities of the surrounding water and air, current and wind velocities and the acceleration of gravity. The simulated physical domain can be restricted by static boundaries, if the objective of the user is to simulate an operation close to a coastline, or a model-scale experiment in a restricted ice tank.

Both full-scale and model-scale ice covers can be modelled in SIBIS. An example of a model-scale ice field is shown in Figure 2, and the corresponding floe size distribution is shown in Figure 3. An example of a full-scale broken ice field is presented later in this paper.

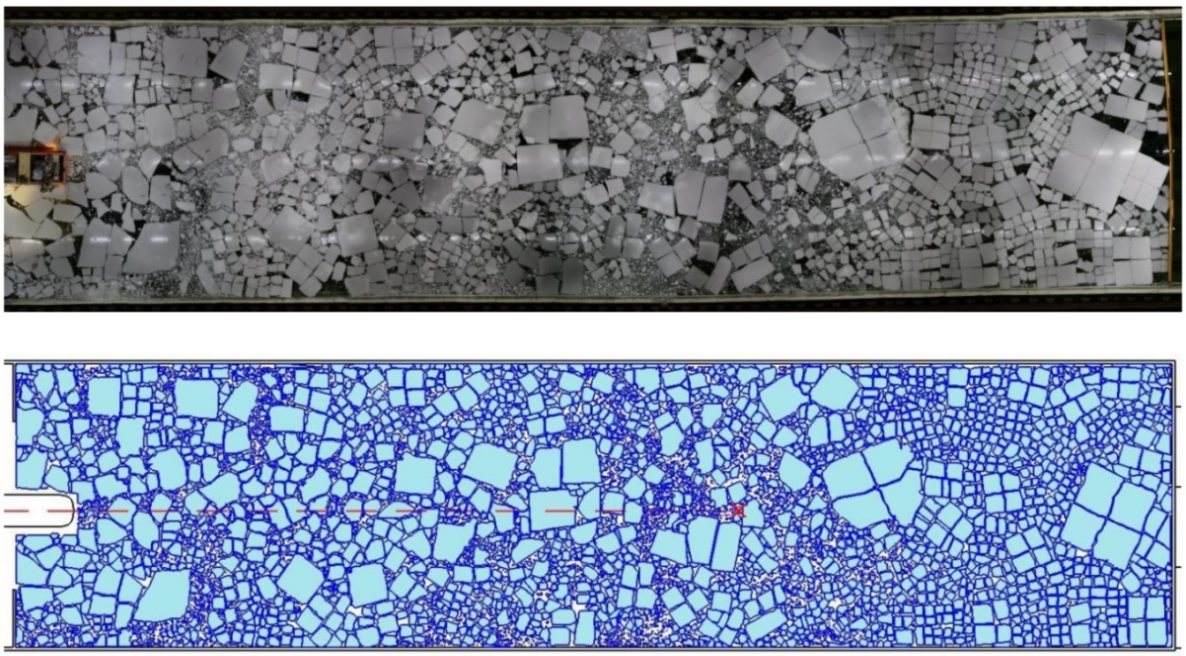

Figure 2. Top: broken ice field picture from the large ice tank of the Hamburg Ship Model Basin (HSVA), bottom: the corresponding ice field input to SIBIS.

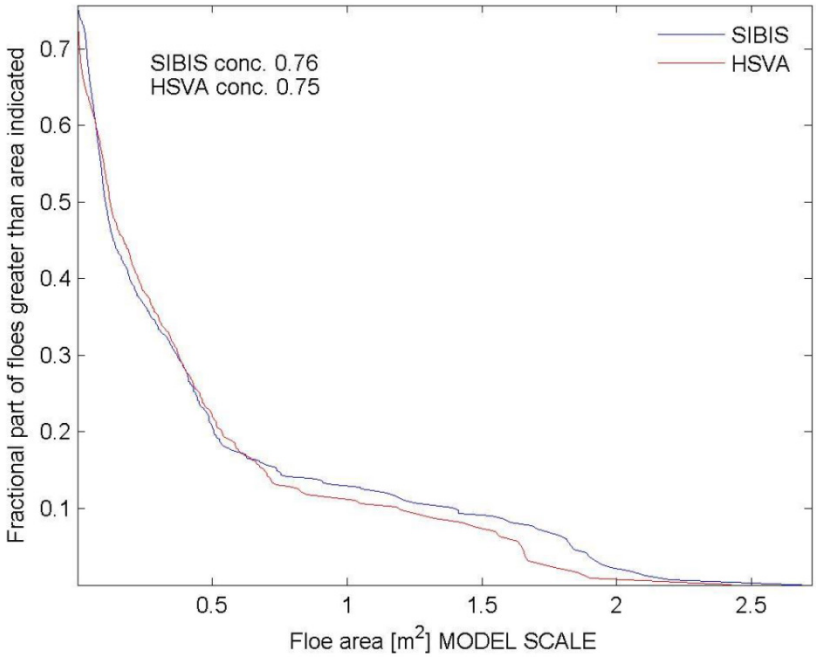

Figure 3. Comparison of floe size distributions from the two images in Figure 2.

The simulated ice cover in SIBIS is composed of individual ice fragments that respond in 6 degrees of freedom (DOF) to accurate fully-nonlinear hydrostatic forces, skin and form drag forces, damping loads and contact forces from other ice floes, structures or boundaries in the simulation domain. Each ice fragment is characterized by a set of individual physical properties (geometry, density, flexural and compressive strengths, Young's modulus, Poisson's ratio and friction coefficients). Therefore, it is possible to simulate ridge fragments and rubble fields in the ice cover, as well as multiyear or glacial ice inclusions. Furthermore, it is possible to assign statistical distributions to all individual properties of the simulated ice floes: both geometrical properties, such as the size and shape of the ice fragments, as well as mechanical properties such as the ice strength.

In every ice-ice contact the pressure and frictional forces are calculated, and possible crushing and rafting processes between the ice floes are modelled. Furthermore, in the ice-structure contacts the ice crushing is taken into account, and the ice floes can fracture in bending and splitting modes against the structural interface. The other simulated loads on the structure include buoyancy, wind and current drag forces, damping loads, mooring reactions and propulsion forces.

Given initial and boundary conditions, the SIBIS simulation engine computes for each time step the dynamics of the ice and the structure in 6 DOF, normal and frictional contact forces for ice-structure and ice-ice interactions, fluid-structure and fluid-ice interactions (hydrostatics and hydrodynamics) and the stationkeeping system behaviour and response. Ice fractures are modelled dynamically, depending on the actual physical configuration of the simulated system at each time step, i.e. the failure patterns are not pre-assumed.

Throughout the simulation process the SIBIS software produces output files with loads on the structure (global and local), motions of the structure, and other relevant numerical data - for subsequent analysis and post-processing by the user. Finally, visualization of the simulation process can be performed by the SIBIS package both in real-time and after full completion of an individual simulation run.

SIBIS MODEL CALIBRATION

The SIBIS model has been calibrated against model-scale experiments of a floating drillship in managed ice conditions at the large ice tank of the Hamburg Ship Model Basin (Bonnemaire et al., 2015). A principle sketch of the corresponding numerical setup is shown in Figure 4: the vessel was moored to an underwater carriage moving forward along the basin, which was modelled with 4 static walls confining the ice cover. The simulated broken ice fields had a similar concentration and floe size distributions as the ones utilized in the model basin. A total of eight interactions performed in the ice basin were modelled numerically. This included ice covers of two different significant floe sizes, two ice thicknesses, and concentrations in the range from 70% to 90%. Special attention was paid to accurate replication and control of the initial ice floe size distributions, because it was one of the main steering parameters in the physical experiments.

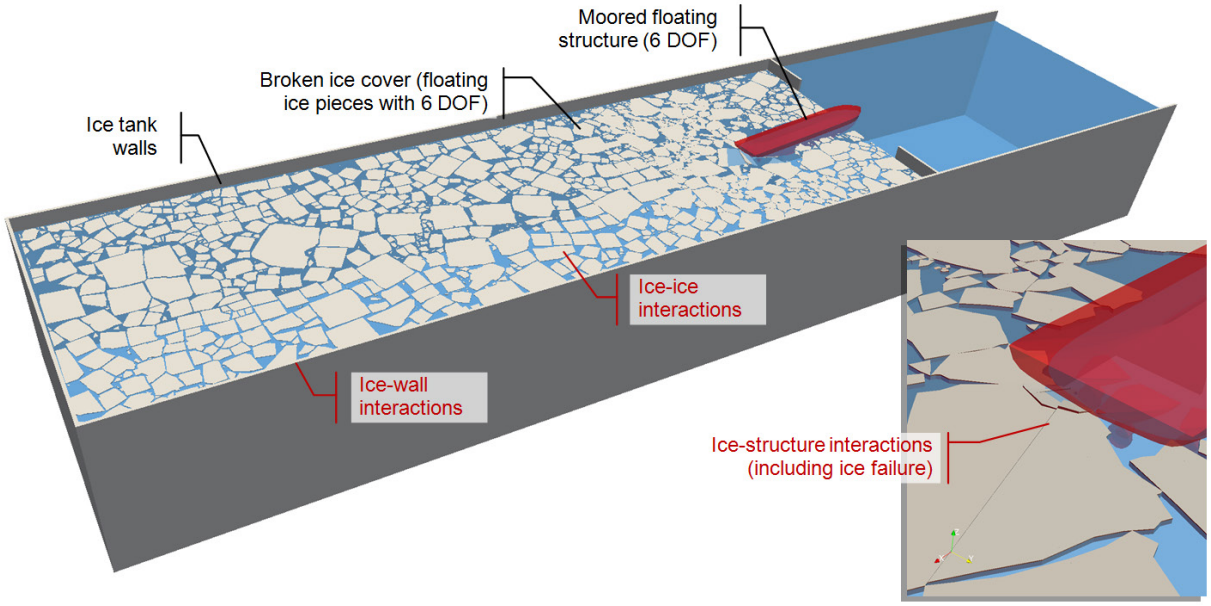

Figure 4. Principle sketch of the SIBIS numerical setup for ice basin simulations.

The outcomes of the simulations were recorded and compared with the available model-scale data. Main focus was placed on the major processes that govern the global response level:

- Response of the ice field, including mobilization of the ice field, confinement increase due to the boundary effects and interlocking effects (Figure 5);
- Ice failure modes (bending, splitting, crushing), ice accumulation and material transport processes around the structure – both in-plane and sub-surface;
- Response of the structure in different degrees of freedom;
- Loads in the mooring system.

Figure 6 shows two examples of comparisons between the achieved and simulated mooring loads. The experimental results are shown in red colour, while the numerical results are shown in blue colour. The load time series indicate that similar mooring load levels and trends are achieved along the ice basin. However, the time series differ locally. Exact replica is not expected due to the nature of interactions in broken ice. Those interactions are highly stochastic, and a small perturbation at some point may evolve into a substantially different global interaction. Furthermore, the interactions are short with just a few main oscillations. Therefore, it is challenging to compare the extreme values since several oscillations (or a longer interaction) may result in completely different extreme values.

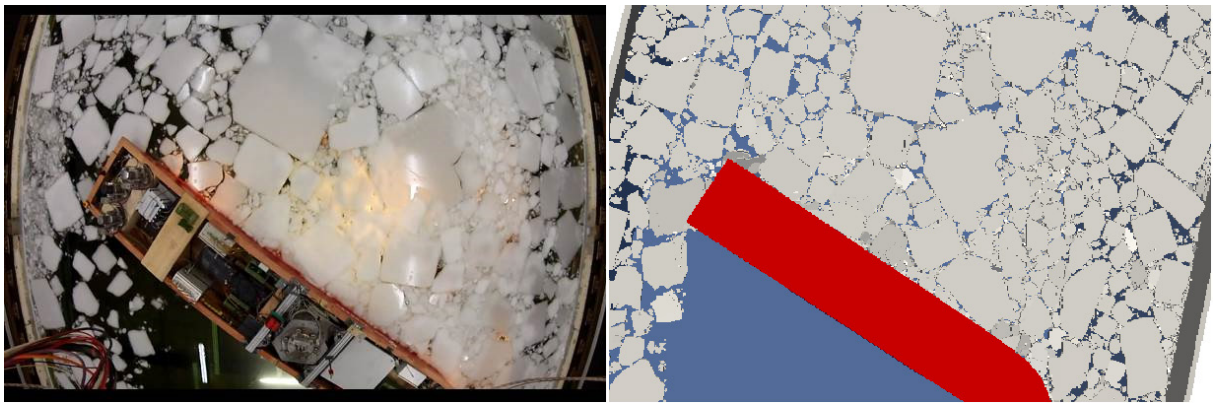

Figure 5. A comparison between ice interactions in the experiment and SIBIS simulation.

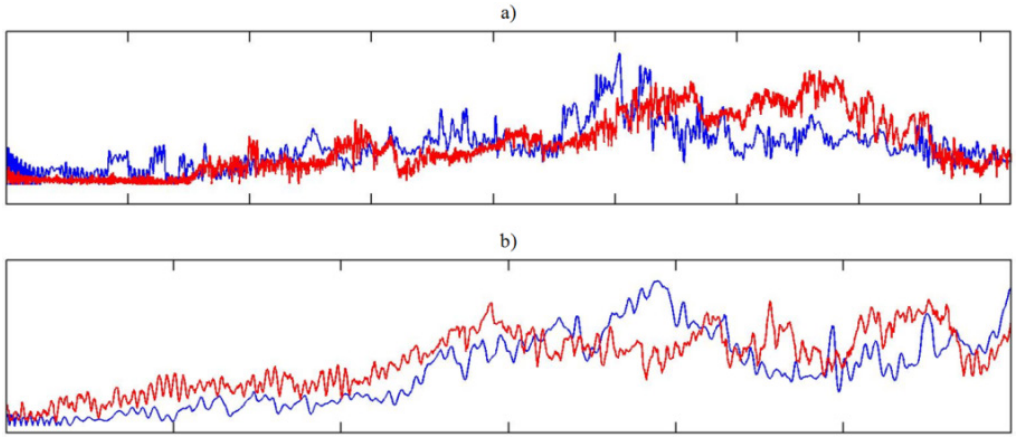

Figure 6. Comparison of the measured (in red) and simulated (in blue) mooring load time series for 2 distinct interactions: a) 90 % concentration, large floes; b) 90 % concentration, small floes. The axes in the plots are not marked due to confidentiality restrictions.

The model-scale results have also been used to calibrate the ice material accumulation and transport functionality in SIBIS. Figure 7 (middle row) qualitatively compares the simulated ice accumulation to the one achieved in the model tests (top row). Pre-broken rectangular ice pieces with a certain thickness were used in the numerical model to reproduce an ice sheet that would lead to ice accumulation. An ice basin configuration was used in SIBIS to tow the stern of the vessel through the ice field at a certain velocity, when the ice field was confined by the walls of the model tank. It can be seen in Figure 7 that the accumulation effects are quite well replicated by the SIBIS model.

SIBIS MODEL APPLICATION

After the numerical model had been calibrated against model-scale experimental data, it was applied for performance assessments of the vessel in realistic metocean conditions (Metrikin et al., 2015). First of all, the SIBIS model was used to evaluate a design change of the icebreaking stern of the vessel. In order to reduce the ice accumulations observed in the model tests, the thruster boxes were modified in an attempt to reduce the ice accumulations and cater for better ice material clearing in the stern area. The boxes were narrowed down and were extended deeper to provide more space for the ice clearing. Then, numerical simulations were performed with the SIBIS model in 180º and 165º astern configurations in 0.6 m and 1.2 m ice thicknesses, and it was verified that the modified stern has enhanced the ice clearing capabilities of the drillship (Figure 7, bottom row). Further material transport investigations could also be performed using the SIBIS model, in order to understand if the ice could be potentially transported into the moonpool of the drillship or foul its mooring lines.

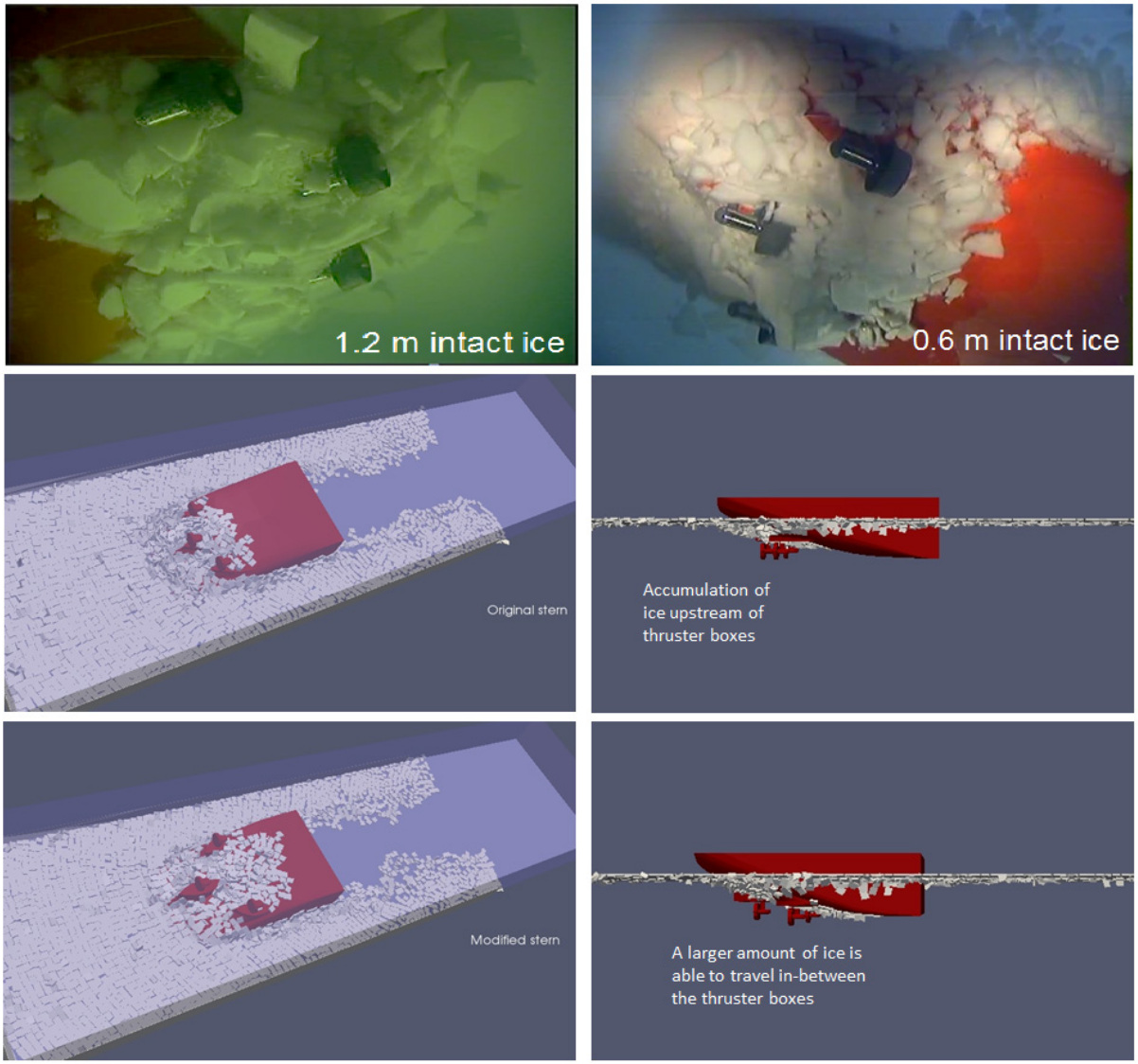

Figure 7. Measurements and simulations of the ice material accumulation and transportation processes. Top row: physical model test, middle row: SIBIS simulation with the original stern design, bottom row: SIBIS simulation with the improved stern design.

The second application of the qualified SIBIS model was to produce a mapping of the vessel's response to a set of interactions with realistic full-scale managed ice conditions, i.e. development of an M2L (Managed ice to Load) transfer function (Liferov, 2014). This included:

- Definition and modelling of a set of relevant full-scale managed ice environments;
- Simulation of the response of the hull when moored in the drifting ice fields;
- Mapping the response of the vessel to a set of ice conditions (ice floe size distributions, concentrations and thicknesses).

The outcome of the study could then be used to simulate operations at a particular geographical location, and estimate the operability and potential downtime of the drillship at that location.

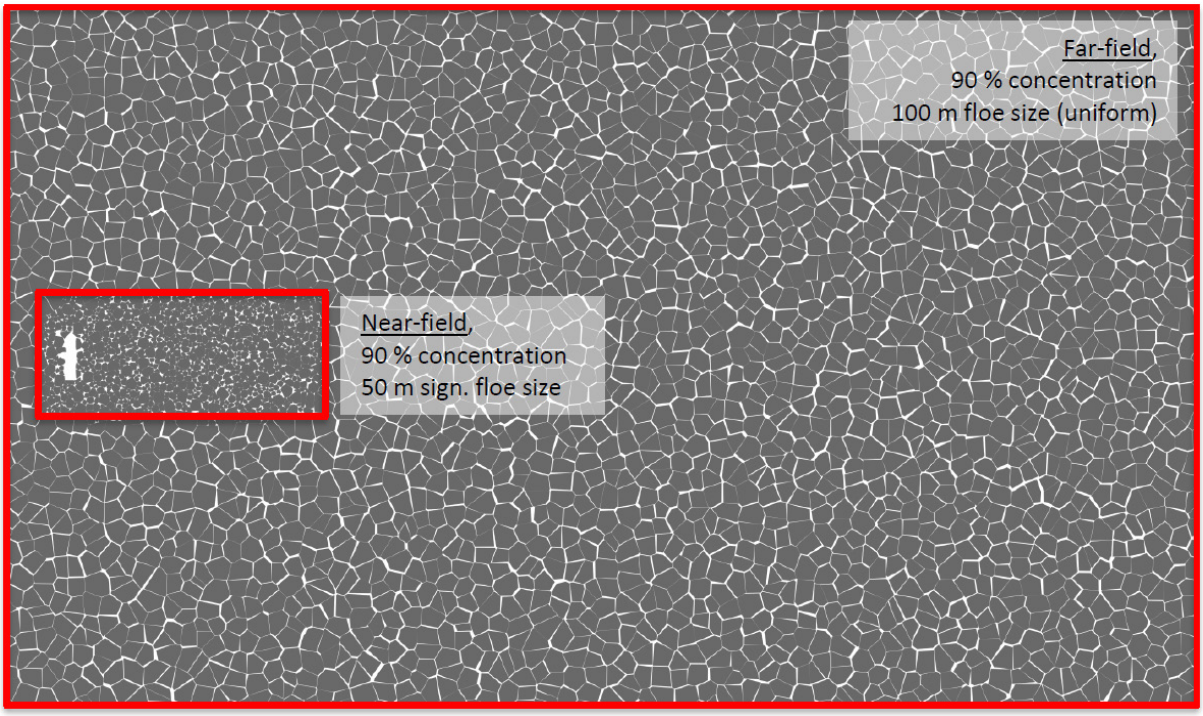

Figure 8. A full-scale managed ice field used for simulations in SIBIS.

The broken ice fields used in the simulations were divided into two parts: a near-field area of managed ice and a far-field area where the floes were unmanaged. The ice concentration was the same over the whole ice field (both near-field and far-field), ensuring a uniform confinement over the whole ice cover. An example of the utilized ice field is shown in Figure 8, where the simulation domain is 6000m long and 3500m wide, and the near-field managed ice domain dimensions are 1500m by 700m. The corresponding simulation setup in SIBIS is shown in Figure 9, and several snapshots from the dynamical simulation process are shown in Figure 10. Finally, an example of simulation results is given in Figure 11.

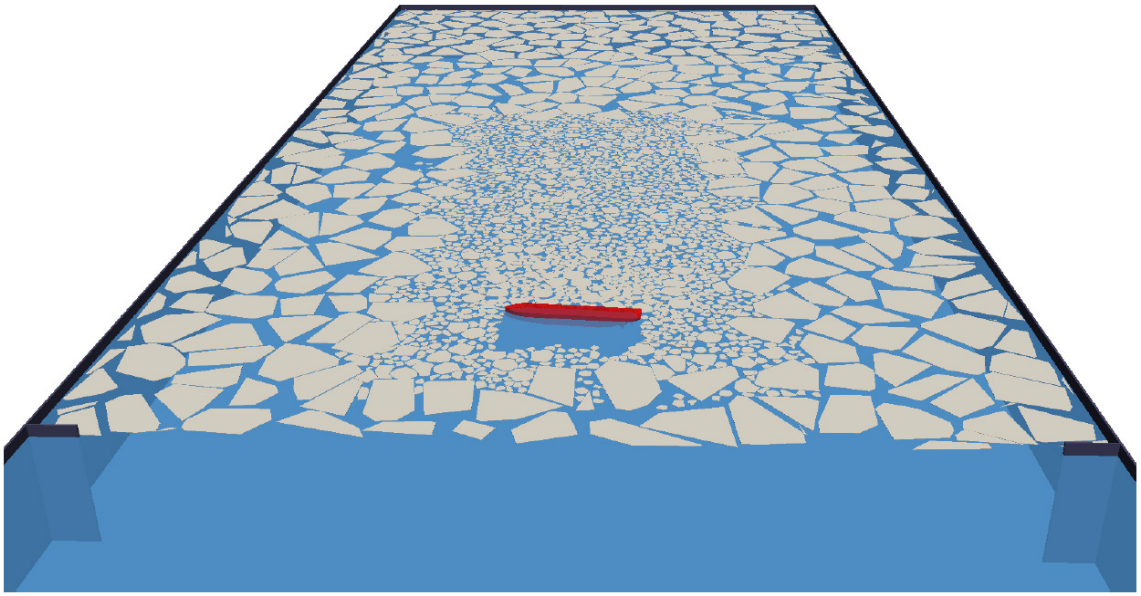

Figure 9. SIBIS simulation setup for a vessel in managed ice.

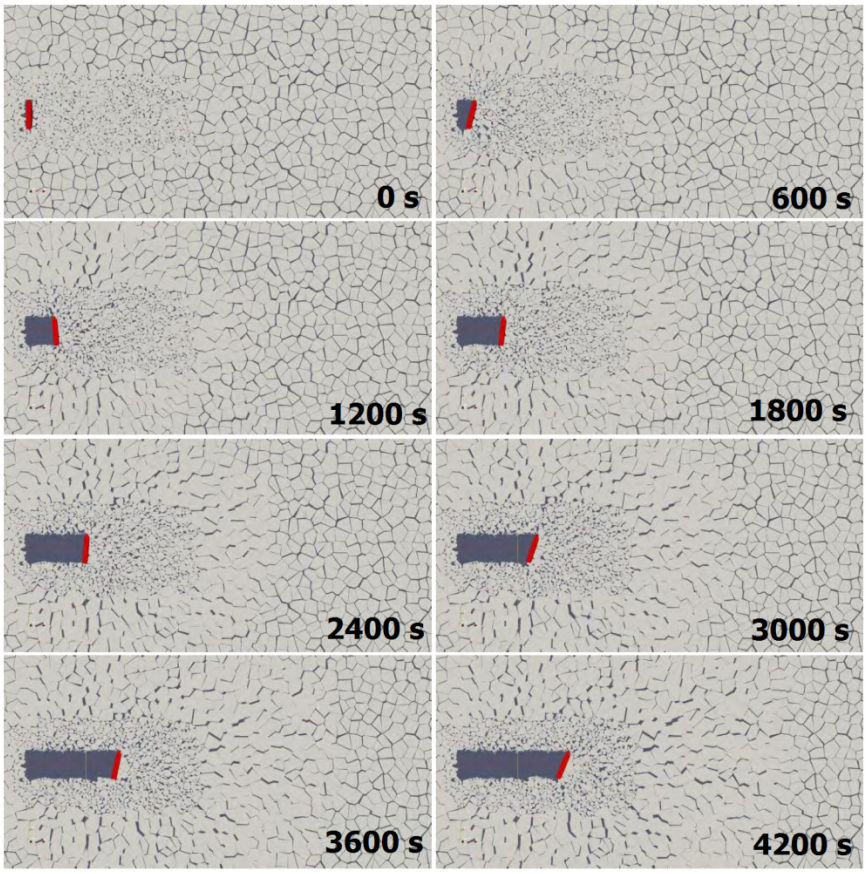

Figure 10. Bird-view snapshots from a SIBIS simulation in 90% ice concentration with 50m significant floe size and 0.5m thick ice floes (90° initial ice drift heading).

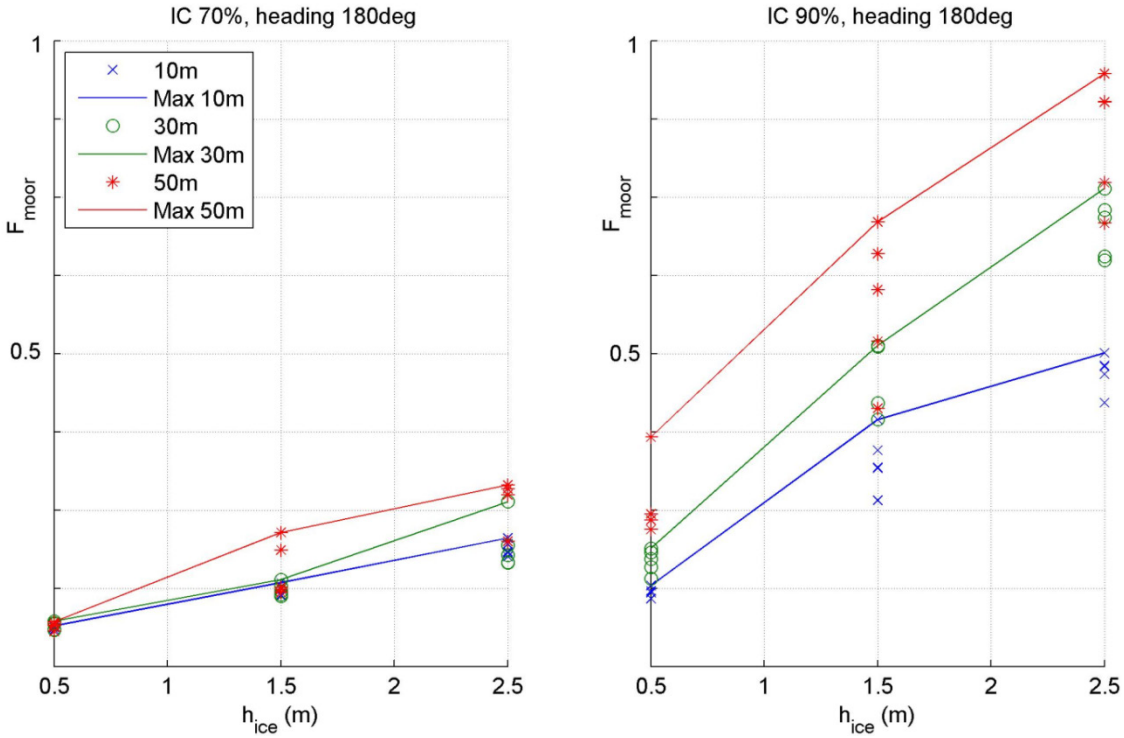

Figure 11. Maximum mooring loads (normalized) for 180° initial heading. Each dot is for one run of each scenario: ice concentration and floe size distribution are constant, but the geometrical positions of the floes are rearranged. 10m, 30m and 50m are the managed ice floe sizes. The continuous lines show the upper-bound envelopes of the mooring loads.

It can be seen in Figure 11 that the mooring loads increase almost linearly with the ice thickness. However, the load levels are 2 – 3 times higher at 90% ice concentration compared to 70% ice concentration. Furthermore, the load levels are 1.5 – 2 times larger for 50m ice floes compared to 10m ice floes. These trends are expected, and were confirmed to be in accordance with existing empirical formulations for managed ice loads on floating structures.

DISCUSSION

Interaction between a floating structure and a broken ice field is a complex process due to the highly nonlinear interdependency between the ice actions and the structural response. It is also a highly stochastic process, because the bearing capacity of the broken ice cover depends on the distribution and shapes of a large amount of individual ice fragments. Therefore, a small perturbation of an individual interaction event (e.g. rotation of an ice floe instead of fracture) may lead to a substantially different response of the ice cover in the long term, which in turn will lead to a different global action on the structure. Those properties are challenging with regards to both repeatability of a given interaction and estimation of the statistical parameters of a response time series (such as expected extremes). Therefore, a full replication of the ice-structure interaction process does not seem to be possible, and some deviations are perhaps unavoidable. Due to the stochastic character of the interactions, the measured and simulated responses should then be compared only with regards to trends, load levels and general dependencies on the structural response or the boundary conditions.

The SIBIS numerical model is a good tool for simulating such complex interactions, because it captures the dynamical behaviour of the structure in all degrees of freedom (e.g. roll and pitch angles affecting the waterline and the associated local ice-structure interaction, and the yaw angle affecting the relative ice drift direction) as well as the ice field dynamics, including compaction, interlocking, formation of accumulations, ice transport effects, fracture of ice floes, friction, fluid effects etc. However, realistic simulations require a sufficiently precise numerical replica of the broken ice field (especially with regards to the ice concentration and floe size distribution), because even slight perturbations in the ice field may lead to significant disturbances of the load and response signals (as can be seen in Figure 11). Further investigations of those perturbations and a rigorous statistical analysis of the simulation results are subject to further research work with the SIBIS model. Furthermore, image processing methods for identification and extraction of individual ice floes and representative floe size distributions (Zhang and Skjetne, 2014a, 2014b; Zhang et al., 2015) are highly relevant to the problems discussed in this paper, and should be further explored.

The main limitation of the current SIBIS model is the lack of validation against full-scale data. Therefore, there is currently an ongoing validation effort against the publically available Kulluk dataset, and additional dedicated full-scale measurements are being collected in Statoil-led expeditions and field trials for the purpose of validating SIBIS. Furthermore, the hydrodynamic model of SIBIS is currently being re-developed in order to include the added mass effects and a better numerical model for the damping loads. One of the ambitions with regards to hydrodynamics is to include functionalities for simulating waves in the broken ice field and combined wave-ice actions on offshore structures. Additionally, there is a need to develop an ice drift feature which would produce realistic motions of a broken ice field under the influence of winds and currents. With regards to ice mechanics, there is a need to develop a better brash ice model, functionality for ridge building in ice-ice contacts, and a model for consolidated ice rubble (e.g. cohesion in the keels of ice ridges). Finally, there is an on-going effort to improve the computational efficiency of the software by utilizing GPU parallelization and cloud computing technologies.

CONCLUSIONS

This paper presents a novel, independently developed numerical environment for simulating offshore operations in discontinuous ice – SIBIS (**S**imulation of **I**nteraction between **B**roken **I**ce and **S**tructures). The structure and capabilities of the software package are described in the paper, together with the input-output functionalities available to the user. Furthermore, calibrations of the numerical model against model-scale experiments of a floating drillship in broken ice conditions, described in the paper, demonstrate that SIBIS produces adequate results which can be used for preliminary performance assessments of the drillship's operability in broken ice conditions. Application examples of the calibrated model include a design change of the hull structure of the drillship, and mapping of the vessel's response to a set of interactions with realistic managed ice fields. In the latter example it is found that the global load trends, produced by SIBIS, are reasonable and in accordance with existing empirical formulations for global loads on floating structures from broken ice. Finally, some limitations of the numerical model are indicated and further development efforts are outlined.

ACKNOWLEDGEMENTS

The authors would like to thank Jørgen Jorde and the whole expert team of Inocean for a very good collaboration experience within the Cat I project. Furthermore, the authors would like to acknowledge Alexander Saue, Eirik Strøm Uthaug, Elisabeth Hostrup, Espen Jørgensen, Pavel Liferov, Sigurd Henrik Teigen and Xinying Zhu from Statoil; Christian Schröder, Jens-Holger Hellmann and the whole ice tank crew of HSVA; Sofien Kerkeni from Sirehna; and Arnor Jensen, Nicolas Serré, Trine Lundamo and Åse Ervik from Multiconsult for their support, assistance, dedication and trust.

REFERENCES

Alawneh, S., 2014. Hyper-Real-Time Ice Simulation and Modeling Using GPGPU. PhD thesis. Memorial University of Newfoundland.

Alawneh, S., Dragt, R., Peters, D., Daley, C., G., Bruneau, S., 2015. Hyper-Real-Time Ice Simulation and Modeling Using GPGPU. IEEE Transactions on Computers. doi:10.1109/TC.2015.2409861.

Amdahl, T., H., Bjørnsen, B., Hagen, O., J., Søberg, S., R., 2014. Numerical simulations of ice loads on an Arctic Floater in managed ice. Arctic Technology Conference, 10-12 February 2014, OTC paper number 24549, doi:10.4043/24549-MS.

Barker, A., Sayed, M., Timco, G., W., 2000. Numerical Simulations of Broken Ice Interaction with Structures. National Research Council of Canada, Canadian Hydraulics Centre Technical Report HYD-TR-050, PERD/CHC Report 9-82.

Barker, A., Sayed, M., Timco, G., W., 2002. Numerical Simulation of Ice Interaction with a Wide Cylindrical Pier. Cold Regions Engineering Conference, pp. 617-628.

Barker, A., Sayed, M., 2012. Upward- or Downward-Breaking Cones in Ice: Which One Should You Use? Cold Regions Engineering Conference, pp. 715-724.

Barker, A., Sudom, D., Sayed, M., 2014. Conical structures in ice: the roles friction, slope and shape play. Arctic Technology Conference, 10-12 February 2014, OTC paper number 24566, doi:10.4043/24566-MS.

Bonnemaire, B., Tan, X., Serré, N., Fredriksen, A., Metrikin, I., Gürtner, A., 2015. Post-simulations of Ice Basin Tests of a Moored Structure in Broken Ice - Challenges and Solutions. Arctic Technology Conference, 23-25 March 2015, OTC paper number 25531, doi:10.4043/25531-MS.

Croasdale, K., R., Bruce J., R., Liferov, P., 2009. Sea Ice Loads Due To Managed Ice. 20th International Conference on Port and Ocean Engineering under Arctic Conditions (POAC'09). June 9-12, 2009, Luleå, Sweden.

Cundall, P., A., 1971. A computer model for simulating progressive, large-scale movements in blocky rock systems. Symposium of the International Society for Rock Mechanics, 2(8), pp. 129-136.

Daley, C., G., Alawneh, S., Peters, D., Quinton, B., W., Colbourne, D., B., 2012. GPU Modeling of Ship Operations in Pack Ice. International Conference and Exhibition on Performance of Ships and Structures in Ice (ICETECH 2012).

Daley, C., G., Alawneh, S., Peters, D., Blades, G., Colbourne, B., 2014a. Simulation of Managed Sea Ice Loads on a Floating Offshore Platform using GPU-Event Mechanics. International Conference and Exhibition on Performance of Ships and Structures in Ice (ICETECH 2014).

Daley, C., G., Alawneh, S., Peters, D., Colbourne, B., 2014b. GPU-Event-Mechanics Evaluation of Ice Impact Load Statistics. Arctic Technology Conference, 10-12 February 2014, OTC paper number 24645, doi:10.4043/24645-MS.

Eik, K., J., Aksnes, V., Ø., 2010. Characterisation of peak loads on a moored production vessel in ice. 20th IAHR International Symposium on Ice, Lahti, Finland, June 14 to 18, 2010.

Eik, K., J., 2011. Sea-ice management and its impact on the design of offshore structures. Cold Regions Science and Technology, 65(2), 172–183. doi:10.1016/j.coldregions.2010.10.009.

Gürtner, A., Bjørnsen, B., E., Amdahl, T., H., Søberg, S., R., Teigen, S., H., 2012. Numerical Simulations of Managed Ice Loads on a Moored Arctic Drillship. Arctic Technology Conference, 3-5 December 2012, OTC paper number 23816, doi:10.4043/24549-MS.

Haase, A., Polojärvi, A., Tuhkuri, J., 2010. 3D Discrete Numerical Modelling of Conical Structure-Ice Rubble Interaction. IAHR International Symposium on Ice, pp. 330-335.

Hals, T., Jenssen, N., A., 2012. DP ice model test of arctic drillship and polar research vessel. International Conference on Offshore Mechanics and Arctic Engineering (OMAE2012), vol. 6, pp. 467–472.

Ishibashi, D., Shigihara, T., Konno, A., 2014. Experimental and Numerical Investigation of Model-Scale Collision of Ship with Ice Floe. 22nd IAHR International Symposium on Ice, pp. 495–502.

Iyerusalimskiy, A., Gu, G., Zou, J., Chianis, J., Kumar, B., Sayed, M., 2012. A conceptual study of deepwater arctic floater for year-round drilling and production. International Conference and Exhibition on Performance of Ships and Structures in Ice (ICETECH 2012).

Jenssen, N., A., Muddusetti, S., Phillips, D., Backström, K., 2009. Dynamic Positioning in Ice Conditions. Dynamic Positioning Conference 2009. Houston, Texas, USA.

Jenssen, N., A., Hals, T., Jochmann, P., Haase, A., Dal Santo, X., Kerkeni, S., Doucy, O., Gürtner, A., Støle Hetschel, S., Moslet, P., O., Metrikin, I., Løset, S., 2012. DYPIC - A Multi-National R&D Project on DP Technology in Ice. Dynamic Positioning Conference 2012. Houston, Texas, USA.

Ji, S., Li, Z., Li, C., Shang, J., 2013. Discrete element modeling of ice loads on ship hulls in broken ice fields. Acta Oceanologica Sinica, 32(11), 50–58. doi:10.1007/s13131-013-0377-2.

Ji, S., P., Li, Z., L., Huang, M., M., Wang, Y., H., Tian, Y., K., Li, Z., G., 2014. Initial concept design for a self-icebreaking container vessel in ice-covered water region. International Offshore and Polar Engineering Conference (ISOPE2014), pp. 1144-1151.

Karulin, E., B., Karulina, M., M., 2010. Performance Studies for Technological Complex Platform “Prirazlomnaya” – Moored Tanker in Ice Conditions. Ninth (2010) ISOPE Pacific/Asia Offshore Mechanics Symposium, Busan, South Korea, pp. 202–208.

Karulin, E., B., Karulina, M., M., 2011. Numerical and physical simulations of moored tanker behaviour. Ships and Offshore Structures, 6(3), 179–184. doi:10.1080/17445302.2010.544087.

Karulin, E., B., Karulina, M., M., 2013. Determination of loads on mooring system during the semisubmersible interaction with ice. International Offshore and Polar Engineering Conference (ISOPE2013), pp. 1288–1294

Karulin, E., B., Karulina, M., M., 2014. Peculiarities of Multi-Legged Platform Operation in Ice Condition. In ASME 2014 33rd International Conference on Ocean, Offshore and Arctic Engineering (ISOPE2014), June 8-13, 2014, San Francisco, California, USA.

Keinonen, A., J., Browne, R., Revill, C., Reynolds, A., Robbins, I., 1998. Icebreaker Characteristics Synthesis. Transport Canada Transportation Development Centre Technical Report No. TP 12812E, in 3 volumes. AKAC INC.

Kerkeni, S., Dal Santo, X., Metrikin, I., 2013a. Dynamic Positioning in Ice - comparison of control laws in open water and ice. ASME 2013 32nd International Conference on Ocean, Offshore and Arctic Engineering (OMAE2013).

Kerkeni, S., Metrikin, I., Jochmann, P., 2013b. Capability Plots of Dynamic Positioning in Ice. ASME 2013 32nd International Conference on Ocean, Offshore and Arctic Engineering (OMAE2013).

Kerkeni, S., Metrikin, I., 2013. Automatic Heading Control for Dynamic Positioning in Ice. Dynamic Positioning Conference 2013, Houston, Texas, USA.

Kim, M.-C., Lee, S.-K., Lee, W.-J., Wang, J., 2013. Numerical and experimental investigation of the resistance performance of an icebreaking cargo vessel in pack ice conditions. International Journal of Naval Architecture and Ocean Engineering, 5(1), 116–131. doi:10.3744/JNAOE.2013.5.1.116.

Kim, M.-C., Lee, W.-J., Shin, Y.-J., 2014. Comparative study on the resistance performance of an icebreaking cargo vessel according to the variation of waterline angles in pack ice conditions. International Journal of Naval Architecture and Ocean Engineering, 6, 876–893. doi:10.2478/IJNAOE-2013-0219.

Kjerstad, Ø., K., Skjetne, R., 2014. Modeling and Control for Dynamic Positioned Marine Vessels in Drifting Managed Sea Ice. Modeling, Identification and Control: A Norwegian Research Bulletin, 35(4), 249–262. doi:10.4173/mic.2014.4.3.

Kjerstad, Ø., K., Metrikin, I., Skjetne, R., 2015. Description and Numerical Simulations of Dynamic Positioning in Reversing Managed Ice. 23rd International Conference on Port and Ocean Engineering under Arctic Conditions (POAC'15).

Konno, A., Mizuki, T., 2006a. On the numerical analysis of flow around ice piece moving near icebreaker hull (Second report: Application of Physically-Based Modeling to simulation of ice movement). 21st International Symposium on Okhotsk Sea & Sea Ice, pp. 74-77.

Konno, A., Mizuki, T., 2006b. Numerical Simulation of Pre-Sawn Ice Test of Model Icebreaker Using Physically Based Modeling. Proc. of the 18th IAHR International Symposium on Ice.

Konno, A., Yasuki, N., Yamamoto, K., Wako, D., Takimoto, T., Izumiyama, K., 2007. On the numerical analysis of flow around ice piece moving near icebreaker hull (Third report: comparison of simulation results with experimental results under pre-sawn ice condition). 22nd International Symposium on Okhotsk Sea & Sea Ice, pp. 29–32.

Konno, A., Yoshimoto, K., 2008. Numerical simulation of ship navigation in brash ice channels. 23rd International Symposium on Okhotsk Sea & Sea Ice, pp. 104–107.

Konno, A., 2009a. Numerical simulation of ship navigation in brash ice channels (Second report: effect of size and layer number of ice pieces). 24th International Symposium on Okhotsk Sea & Sea Ice, pp. 35–38.

Konno, A., 2009b. Resistance Evaluation of Ship Navigation in Brash Ice Channels with Physically Based Modeling. 20th International Conference on Port and Ocean Engineering under Arctic Conditions(POAC'09), Luleå, Sweden.

Konno, A., Saitoh, O., 2010. Preparation method of numerical ice channel and its evaluation for simulation of navigation in ice. 25th International Symposium on Okhotsk Sea & Sea Ice, pp. 154–159.

Konno, A., Saitoh, O., Watanabe, Y., 2011. Numerical investigation of effect of channel condition against ship resistance in brash ice channels. 21st International Conference on Port and Ocean Engineering under Arctic Conditions (POAC'11).

Konno, A., Nakane, A., Kanamori, S., 2013. Validation of Numerical Estimation of Brash Ice Channel Resistance with Model Test. 22nd International Conference on Port and Ocean Engineering under Arctic Conditions (POAC'13).

Lau, M., 2006. Discrete Element Modeling of Ship Manoeuvring in Ice. 18th IAHR International Symposium on Ice, pp. 25-32.

Lau, M., Ré, A., S., 2006. Performance of Survival Craft in Ice Environments. International Conference and Exhibition on Performance of Ships and Structures in Ice (ICETECH 2006).

Lau, M., Lawrence, K., P., Rothenburg, L., 2011. Discrete element analysis of ice loads on ships and structures. Ships and Offshore Structures, 6(3), 211–221. doi:10.1080/17445302.2010.544086.

Lawrence, K., P., 2009. Load Prediction for a Moored Conical Drillship in Level Unbroken Ice: A Discrete Element and Experimental Investigation. PhD thesis, University of Waterloo.

Lee, S.-G., Zhao, T., Kim, G.-S., Park, K.-D., 2013. Ice resistance test simulation of arctic cargo vessel using FSI analysis technique. 23rd International Offshore and Polar Engineering Conference (ISOPE 2013), pp. 1162-1168.

Liferov, P., 2014. Station-Keeping in Ice – Normative Requirements and Informative Solutions. Arctic Technology Conference, 10-12 February 2014, OTC paper number 24580, doi:10.4043/24580-MS.

Liu, L., Zhan, D., Spencer, D., Molyneux, D., 2010. Pack ice forces on floating offshore oil and gas exploration systems. International Conference and Exhibition on Performance of Ships and Structures in Ice (ICETECH 2010).

Lobanov, V., A., 2011. Evaluation of Ice Propulsion Ability of Ship by Numerical Methods (in Russian). Differential Equations and Control Processes, (1), 34-47.

Lubbad, R., Løset, S., 2011. A numerical model for real-time simulation of ship–ice interaction. Cold Regions Science and Technology, 65(2), 111–127. doi:10.1016/j.coldregions.2010.09.004.

Lubbad, R., Løset, S., 2015. Time Domain Analysis of Floe Ice Interactions with Floating Structures. Arctic Technology Conference, 23-25 March 2015, OTC paper number 25517, doi:10.4043/25517-MS.

Metrikin, I., Lu, W., Lubbad, R., Løset, S., Kashafutdinov, M., 2012a. Numerical Simulation of a Floater in a Broken-Ice Field: Part I - Model Description. ASME 2012 31st International Conference on Ocean, Offshore and Arctic Engineering (OMAE2012).

Metrikin, I., Borzov, A., Lubbad, R., Løset, S., 2012b. Numerical Simulation of a Floater in a Broken-Ice Field: Part II - Comparative Study of Physics Engines. ASME 2012 31st International Conference on Ocean, Offshore and Arctic Engineering (OMAE2012).

Metrikin, I., Løset, S., Jenssen, N., A., Kerkeni, S., 2013. Numerical Simulation of Dynamic Positioning in Ice. Marine Technology Society Journal, 47(2), 14–30. doi:10.4031/MTSJ.47.2.2.

Metrikin, I., Løset, S., 2013. Nonsmooth 3D Discrete Element Simulation of a Drillship in Discontinuous Ice. 22nd International Conference on Port and Ocean Engineering under Arctic Conditions (POAC'13).

Metrikin, I., 2014. A Software Framework for Simulating Stationkeeping of a Vessel in Discontinuous Ice. Modeling, Identification and Control: A Norwegian Research Bulletin, 35(4), 211–248. doi:10.4173/mic.2014.4.2.

Metrikin, I., Kerkeni, S., Jochmann, P., Løset, S., 2015. Experimental and Numerical Investigation of Dynamic Positioning in Level Ice. Journal of Offshore Mechanics and Arctic Engineering, 137(3), pp. 031501.

Metrikin, I., Teigen, S., H., Gürtner, A., Uthaug, E., S., Sapelnikov, D., Ervik, Å., Fredriksen, A., Lundamo, T., Bonnemaire, B., 2015. Experimental and Numerical Investigations of a Ship-Shaped, Turret-Moored Floating Structure in Intact and Managed Sea Ice Conditions. Arctic Technology Conference, 23-25 March 2015, OTC paper number 25528, doi:10.4043/25528-MS.

Millan, J., Wang, J., 2011. Ice Force Modeling for DP Control Systems. Dynamic Positioning Conference 2011. Houston, Texas, USA.

Molyneux, D., Liu, L., Zhan, D., Reid, G., 2012a. Ice Loads on a Moored Floating Production Unit. 10th International Conference and Exhibition on Performance of Ships and Structures in Ice (ICETECH 2012).

Molyneux, D., Spencer, D., Liu, L., Zhan, D., 2012b. Simulation of Ship Performance in Ice Using a Discrete Element Method. Ice Class Ships Conference (The Royal Institution of Naval Architects.

O'Brien, M., 2004. DECICE and its Applications to Ice-Ship Interactions. National Research Council of Canada, Institute for Ocean Technology Report Number LM-2004-36.

Paavilainen, J., Tuhkuri, J., Polojärvi, A., 2006. Discrete Element Simulation of Ice Pile-Up Against an Inclined Structure. 18th IAHR International Symposium on Ice, Sapporo, Japan, pp. 177–184.

Paavilainen, J., Tuhkuri, J., Polojärvi, A., 2009. 2D combined finite-discrete element method to model multi-fracture of beam structures. Engineering Computations: International Journal for Computer-Aided Engineering, 26(6), 578–598. doi:10.1108/02644400910975397.

Paavilainen, J., Tuhkuri, J., Polojärvi, A., 2010. Rubble pile formation against an inclined structure – analysis of simulation results. 20th IAHR International Symposium on Ice. Lahti, Finland, June 14 to 18, 2010.

Paavilainen, J., Tuhkuri, J., Polojärvi, A., 2011. 2D numerical simulations of ice rubble formation process against an inclined structure. Cold Regions Science and Technology, 68(1-2), 20–34. doi:10.1016/j.coldregions.2011.05.003.

Paavilainen, J., Tuhkuri, J., 2012. Parameter effects on simulated ice rubbling forces on a wide sloping structure. Cold Regions Science and Technology, 81, 1–10. doi:10.1016/j.coldregions.2012.04.005.

Paavilainen, J., 2013. Factors affecting ice loads during the rubbling process using a 2D FE-DE Approach. PhD thesis, Aalto University.

Paavilainen, J., Tuhkuri, J., 2013. Pressure distributions and force chains during simulated ice rubbling against sloped structures. Cold Regions Science and Technology, 85, 157–174. doi:10.1016/j.coldregions.2012.09.005.

Palmer, A., C., Croasdale, K., R., 2013. Arctic Offshore Engineering. World Scientific Publishing Co. Pte. Ltd.

Park, K., D., Chung, Y., K., Jang, Y., S., Kim, H., S., Molyneux, D., 2011. Development of hull forms for a 190,000 DWT icebreaking ore carrier. International Conference on Offshore Mechanics and Arctic Engineering (OMAE2011).

Polojärvi, A., Tuhkuri, J., 2009. 3D discrete numerical modelling of ridge keel punch through tests. Cold Regions Science and Technology, 56(1), 18–29. doi:10.1016/j.coldregions.2008.09.008.

Polojärvi, A., Tuhkuri, J., 2010. Modelling Ridge Keel Freeze Bonds in Finite-Discrete Element Method Simulations. 20th IAHR International Symposium on Ice. Lahti, Finland, June 14 to 18, 2010.

Polojärvi, A., Tuhkuri, J., Korkalo, O., 2012. Comparison and analysis of experimental and virtual laboratory scale punch through tests. Cold Regions Science and Technology, 81, 11–25. doi:10.1016/j.coldregions.2012.04.008.

Polojärvi, A., Tuhkuri, J., 2013. On modeling cohesive ridge keel punch through tests with a combined finite-discrete element method. Cold Regions Science and Technology, 85, 191–205. doi:10.1016/j.coldregions.2012.09.013.

Polojärvi, A., 2013. Sea ice ridge keel punch through experiments: model experiments and numerical modeling with discrete and combined finite-discrete element methods. PhD thesis, Aalto University.

Polojärvi, A., Tuhkuri, J., 2014. 3D DEM for Freeze Bonded Ice Rubble Consisting of Polyhedral Blocks. 22nd IAHR International Symposium on Ice, pp. 195–202.

Polojärvi, A., Tuhkuri, J., Pustogvar, A., 2015. DEM simulations of direct shear box experiments of ice rubble: Force chains and peak loads. Cold Regions Science and Technology, 116, 12–23. doi:10.1016/j.coldregions.2015.03.011.

Quinton, B., W., 2006. DECICE Implementation of Ship Performance in Ice: a Summary Report. National Research Council of Canada, Institute for Ocean Technology Report Number SR-2006-06.

Ranta, J., Tuhkuri, J., Polojärvi, A., Paavilainen, J., 2014. Statistical Reconstruction of Peak Ice Load Data Based on 2D Combined Finite-Discrete Element Method Simulations of Ice Interactions Against Inclined Wall. 22nd IAHR International Symposium on Ice, pp. 426–433.

Sayed, M., 1997. Discrete And Lattice Models of Floating Ice Covers. International Offshore and Polar Engineering Conference (ISOPE1997), pp. 428-433.

Sayed, M., Barker, A., 2011. Numerical Simulations of Ice Interaction with a Moored Structure. Arctic Technology Conference, 7-9 February 2011, OTC paper number 22101, doi:10.4043/22101-MS.

Sayed, M., Kubat, I., 2011. Forces on ships transiting pressured ice covers. International Offshore and Polar Engineering Conference (ISOPE2011), pp. 1087-1092.

Sayed, M., Kubat, I., Wright, B., Iyerusalimskiy, A., Phadke, A., C., Hall, B., K., 2012a. Numerical Simulations of Ice Interaction with a Moored Structure. 10th International Conference and Exhibition on Performance of Ships and Structures in Ice (ICETECH 2012).

Sayed, M., Kubat, I., Wright, B., 2012b. Numerical Simulations of ice forces on the Kulluk: the role of ice confinement, ice pressure and ice management. Arctic Technology Conference, 3-5 December 2012, OTC paper number 23823, doi:10.4043/23823-MS.

Sayed, M., Kubat, I., Wright, B., Millan, J., 2014a. Numerical Simulations of Ice Forces on Moored and Thruster-Assisted Drillships. Arctic Technology Conference, 10-12 February 2014, OTC paper number 24647, doi:10.4043/24647-MS.

Sayed, M., Kubat, I., Wright, B., Millan, J., 2014b. Numerical Modelling of the Stationkeeping of Drillships in Ice. International Conference and Exhibition on Performance of Ships and Structures in Ice (ICETECH 2014).

Sayed, M., Kubat, I., Watson, D., Wright, B., Gash, R., Millan, J., 2015. Simulations of the Stationkeeping of Drillships under Changing Direction of Ice Movement. Arctic Technology Conference, 23-25 March 2015, OTC paper number 25565, doi:10.4043/25565-MS.

Scibilia, F., Metrikin, I., Gürtner, A., Teigen, S., H., 2014. Full-Scale Trials and Numerical Modeling of Sea Ice Management in the Greenland Sea. Arctic Technology Conference, 10-12 February 2014, OTC paper number 24643, doi:10.4043/24643-MS.

Selvadurai, A., P., S., 2009. Fragmentation of Ice Sheets during Impact. CMES: Computer Modeling in Engineering & Sciences, 52(3), 259–278. doi:10.3970/cmes.2009.052.259.

Septseault, C., Béal, P.-A., Le Yaouanq, S., Dudal, A., Roberts, B., 2014. A New Ice Simulation Tool Using a Multi-Model Program. Arctic Technology Conference, 10-12 February 2014, OTC paper number 24644, doi:10.4043/24644-MS.

Septseault, C., Béal, P.-A., Le Yaouanq, S., Dudal, A., Roberts, B., 2015. Update on a New Ice Simulation Tool using a Multi-Model Program. Arctic Technology Conference, 23-25 March 2015, OTC paper number 25591, doi:10.4043/25591-MS.

Spencer, D., Molyneux, D., 2009. Predicting Pack Ice Loads on Moored Vessels. Ice Class Vessels Conference (ICSOT 2009), Busan, Korea.

Sun, S., Shen, H. H., 2012. Simulation of pancake ice load on a circular cylinder in a wave and current field. Cold Regions Science and Technology, 78, 31–39. doi:10.1016/j.coldregions.2012.02.003.

Tuhkuri, J., 2005. Discrete Element Simulations in Ice Engineering. 18th Nordic Seminar on Computational Mechanics.

Vachon, G., Sayed, M., Kubat, I., 2012. Methodology for determination of ice management efficiency. 10th International Conference and Exhibition on Performance of Ships and Structures in Ice (ICETECH 2012).

Vroegrijk, E., A., J., 2012. Application of the Discrete Element Method (DEM) on ship-ice interaction. 10th International Conference and Exhibition on Performance of Ships and Structures in Ice (ICETECH 2012).

Wang, B., Daley, C., G., Sayed, M., Liu, J., 2010. Global Ice Loads on Arctic Drillships. International Conference and Exhibition on Performance of Ships and Structures in Ice (ICETECH 2010). Paper No. ICETECH10-120-RF.

Wang, J., Derradji-Aouat, A., 2010. Ship Performance in Broken Ice Floes - Preliminary Numerical Simulations. NRC Institute for Ocean Technology Report TR-2010-24.

Wang, J., Derradji-Aouat, A., 2011. Numerical Assessment for Stationary Structure (Kulluk) in Moving Broken Ice. 21st International Conference on Port and Ocean Engineering under Arctic Conditions (POAC'11).

Watanabe, Y., Konno, A., 2011. Investigation of effect of flow and channel condition against brash ice channel resistance. 26th International Symposium on Okhotsk Sea & Sea Ice, pp. 103–109.

Woolgar, R., C., Colbourne, D., B., 2010. Effects of hull-ice friction coefficient on predictions of pack ice forces for moored offshore vessels. Ocean Engineering, 37(2-3), 296–303. doi:10.1016/j.oceaneng.2009.10.003.

Wright, B., 1999. Evaluation of Full Scale Data for Moored Vessel Station-keeping in Pack Ice (With Reference to Grand Banks Development). PERD/CHC Report 26-200. B. Wright and Associates Ltd.

Zhan, D., Agar, D., He, M., Spencer, D., Molyneux, D., 2010. Numerical Simulation of Ship Maneuvering in Pack Ice. 29th International Conference on Ocean, Offshore and Arctic Engineering (OMAE2010).

Zhan, D., Molyneux, D., 2012. 3-Dimensional Numerical Simulation of Ship Motion in Pack Ice. ASME 2012 31st International Conference on Ocean, Offshore and Arctic Engineering (OMAE2012).

Zhang, Q., Skjetne, R.. 2014a. Image Processing for Identification of Sea-Ice Floes and the Floe Size Distributions. IEEE Transactions on Geoscience and Remote Sensing, doi:10.1109/TGRS.2014.2366640.

Zhang, Q., Skjetne, R., 2014b. Image Techniques for Identifying Sea-Ice Parameters. Modeling, Identification and Control: A Norwegian Research Bulletin, 35(4), 293–301. doi:10.4173/mic.2014.4.6.

Zhang, Q., Skjetne, R., Metrikin, I., Løset, S., 2015. Image processing for ice floe analyses in broken-ice model testing. Cold Regions Science and Technology, 111, 27–38. doi:10.1016/j.coldregions.2014.12.004.

Østhus, V., 2014. Robust Adaptive Control of a Surface Vessel in Managed Ice Using Hybrid Position- and Force Control, MSc thesis, Norwegian University of Science and Technology.

POAC'15
Trondheim, Norway

Proceedings of the 23rd International Conference on
Port and Ocean Engineering under Arctic Conditions
June 14-18, 2015
Trondheim, Norway

CONFINED COMPRESSION TESTS ON SALINE AND FRESH FREEZE-BONDS

Ida Mari Bueide[1,2,3] and Knut Vilhelm Høyland[2]

[1]Multiconsult AS
[2]Sustainable Arctic and Marine and Coastal Technology (SAMCoT), Center for Research-based Innovation (CRI), Norwegian University of Science and Technology, Trondheim, Norway
[3]The University Center on Svalbard (UNIS)

ABSTRACT

Tri-axial compression tests were conducted on freeze-bonds in saline and fresh ice, with the objective to study the internal freeze-bond stresses in relation to increased radial confinement, as well as how to best conduct these experiments. Cylindrical samples with a freeze-bond at 45° were applied radial static confinement and vertical compression at a constant velocity. The chosen variables consisted of confinement, submersion time, initial temperature and salinity. A larger part of the configurations gave increasing freeze-bond stresses for increasing confinement, both when studying the peak and residual stress plots. Mohr-Coulombs failure criterion was applied and the peak stress plots gave estimated cohesion values in the range 0.003 – 0.099 MPa and 16 – 45° (0.28 - 0.78rad) for internal friction. For the residual stresses the cohesion values were approaching zero and internal friction angles were in the range 11 – 37° (0.19 - 0.65rad). In relation to initial temperature the lowest initial temperature of -8.5°C gave the highest cohesion values. And the configurations with fresh samples had a mean cohesion value 30 % higher than for saline.

INTRODUCTION

Developing a material model for an ice ridge is a long term process. The calculation of forces from ice ridges involves both the consolidated layer and the ice rubble. The ice rubble strength derives from the freeze-bonding and interlocking of ice blocks. Experimental investigations on freeze-bonds have been conducted both in the field and the larger part in the laboratory. Most investigations are done on the topic of freeze-bond strength and the parameters influencing it. Helgøy et al. (2013) recently published articles concerning freeze-bond strength and Repetto-Llamazares and Høyland (2011) compared previous articles results on freeze-bond strengths. Figure 1 shows a principle sketch of test set-ups applied in previous tests.

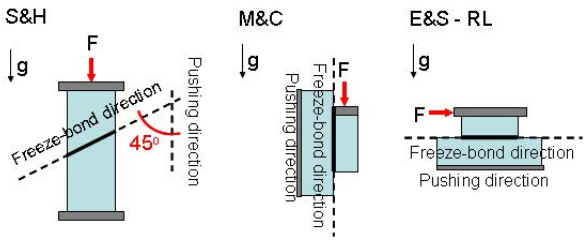

Figure 1. Illustration of experimental set-up from Repetto-Llamazares et al. (2011). S&H- Shafrova and Høyland (2008), M&C- Marchenco and Chenot (2009), E&S- Ettema and Shaefer (1986), RL- Repetto-Llamazares et al. (2011a)

Tri-axial compression tests were conducted on freeze-bonds in saline and fresh ice, with the objective to study the internal freeze-bond stresses in relation to increased radial confinement. Previously this dependency has been investigated by applying loads parallel to the freeze-bond, on top of ice blocks frozen together, as shown in Figure 1 (E&S - RL). A linear increase with increasing confinement has been observed for these experiments and a Mohr-Coulomb failure criterion has been suggested to describe the material. The experiments presented in this paper were conducted in order to investigate this further and to give estimated values of cohesion and internal friction to describe the material strength. The sample dimensions were determined by the devices used. The height of the sample of 150 mm was forced by the dimensions of the pressure clock and the diameter of 70 mm was given by the core sampler kovacs.

EXPERIMENTAL SET-UP

Tri-axial testing was conducted on cylindrical samples with a freeze-bond at 45°, by applying radial static confinement σ_r and vertical compression at a constant velocity. A principal sketch is presented in Figure 2.

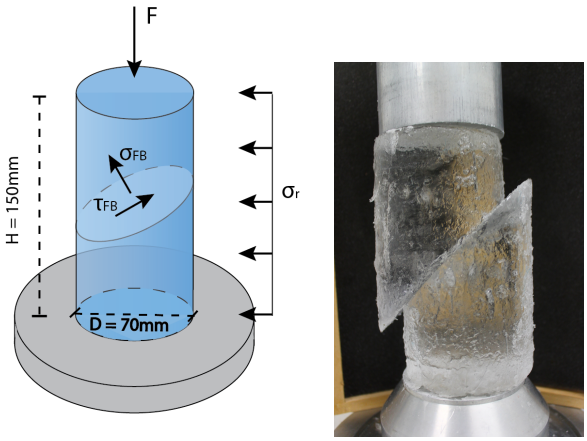

(a) (b)

Figure 2. a) Illustration of experimental set-up b) sample after testing

To prepare for the compression test, pre-cut samples were placed in the Cold-Lab until the ice was in thermal equilibrium with the air temperature, which was set to the desired initial temperature (T_i). The basin used to submerge the samples was also placed in the lab and continuously stirred until the desired temperature (T_w) was reached. The submersion water was set according to the freezing point of the water, -0.5°C for 8ppt and 0.0°C for the fresh water samples.

Firstly the dimensions of the sample was measured and logged before a 45° section was cut with a circular saw. Secondly the sample was assembled in a device called FIXIS, which holds the two cylindrical ice blocks together in a fixed position. This was then immediately submerged for a given time (Δt). The samples were submerged without any confinement. The salinity (S_w) and the temperature (T_w) of the submersion water were measured between each sample. After submersion the sample was removed from the FIXIS and placed in the pressure clock, which was then placed in the compression device. The pressure in the clock was set to the desired confinement value (σ_r) before the piston force was applied with a constant velocity (V).

The deformation limit was constrained by the height of the pressure clock, this sets the limit to 17-20 mm. Deformation (δh) and piston force was logged. After the tests the temperature of the sample ($T_{ice,test}$) was measured, the failure mode was recorded by observation together with relevant comments and pictures were taken. The sample was placed in a container to melt and later the salinity was measured.

Both fresh and saline ice was used in these tests. The fresh ice was collected from Isdammen in Longyearbyen over a period of time. By thin-sections it was defined as an S1 type with average grain size of 9 mm. The density varied between 920kg/m^3 and 941kg/m^3 depending on the air content. This is high, the maximum pure ice density is 917 kg/m^3. The saline samples were produced in the ice production basin FRYSIS at UNIS. A method of seeding as described by Helgøy et al. (2013) was used. The ice was defined as in-between S1 and S3 type and had a salinity of 2.2 - 2.8 ppt.

Test configurations

Four test series were conducted, two with fresh water samples submerged in fresh water and two with saline samples submerged in saline water (figure **??**). Each test series were divided into six configurations, where all were tested with three confinement values σ_r (equation 1). One exemption was made for the fresh water samples with initial temperature of -2.5°C, they were only tested for the two shortest submersion times because of weak freeze-bonds beyond this point.

$$\sigma_r = [0.0070 - 0.0094, 0.0200 - 0.0212, 0.0987 - 0.1026]MPa \quad (1)$$

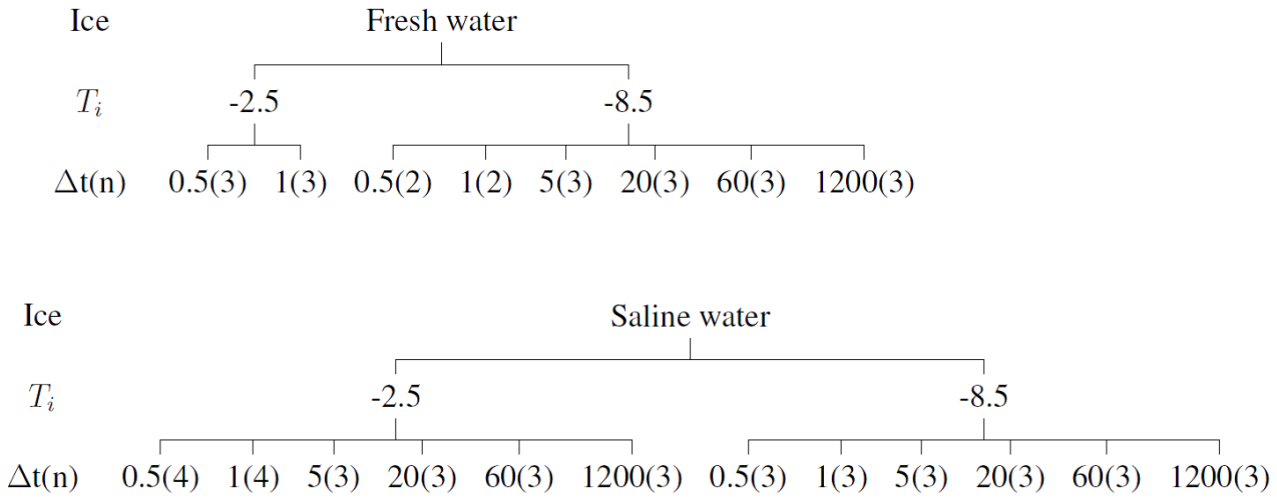

Illustration of test configurations. Ice temperature (T_i), submersion time (Δt) and number of samples (n) tested for each configuration

Force, stresses and velocity

The strength measurements were conducted in the compression machine KNEKKIS applying a vertical force at a constant velocity of 0.8 mm/s corresponding to a sliding velocity of 1.13 mm/s. The radial pressure was obtained by using a pressure clock. With a 45° compression angle relative to the freeze-bond a shear fracture resulting from displacement along this plane was obtained. The output data was an approximately static radial pressure and a time dependent force logged with a time step of 0.1 seconds. The piston force σ_z was defined as the logged force F divided by the circular area of the sample as shown in equation 2. The residual force was defined as the measured force after the peak was reached, divided by the circular area of the sample.

$$\sigma_z = \frac{Measuredpistonforce}{\pi r^2} \tag{2}$$

The peak and residual freeze-bond shear stress was calculated as shown in the appendix. The resulting freeze-bond stresses are shown in equation (3).

$$\begin{aligned} \sigma_{FB} &= \frac{8}{\pi^2}\sigma_r + \sigma_z - \sigma_{FB} \\ &= \frac{4}{\pi^2}\sigma_r + \frac{1}{2}\sigma_z \end{aligned}$$

$$\begin{aligned} \tau_{FB} &= \sigma_z - \frac{4}{\pi^2}\sigma_r - \frac{1}{2}\sigma_z \\ &= \frac{1}{2}\sigma_z - \frac{4}{\pi^2}\sigma_r \end{aligned} \tag{3}$$

These results were used to determine the peak stress dependency for the different parameters, and further to estimate cohesion values and internal friction angles.

PEAK SHEAR STRESS

Results

In Figure 3 the freeze-bond stress τ_{FB} was plotted according to submersion time Δt, the saline experiments in Figure 3 a) and the fresh in 3 b). We found a bell-curve development of the stress vs submersion time, as suggested by Shafrova and Høyland (2008) and found experimentally Repetto-Llamazares et al. (2011). The fresh water samples generally peaked at shorter submersion times than the saline. For the initial temperature of -8.5°C the curve peaked at submersion times of 5 min or less, while for the initial temperature of -2.5°C the curve peaked at submersion times of 1 min or less. For both saline and fresh water samples the peak shear stress increased with decreasing initial temperature.

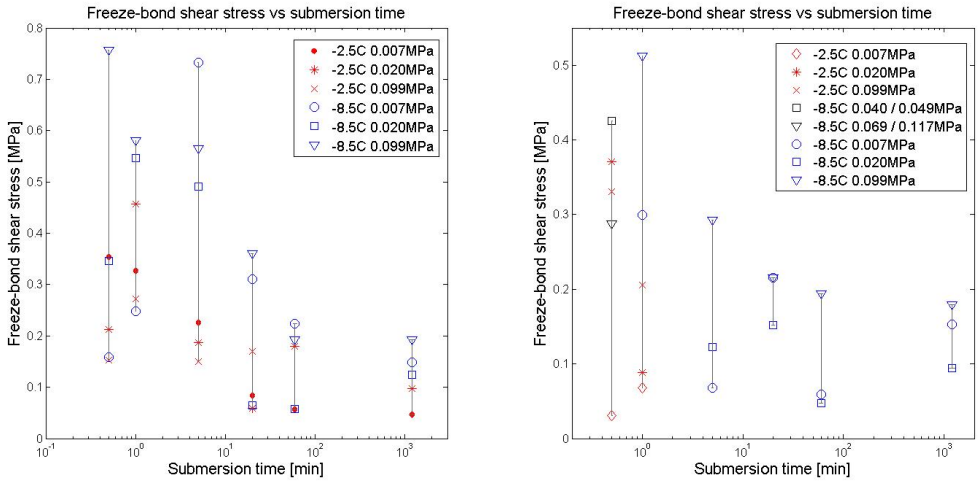

(a) (b)

Figure 3. Submersion time Δt vs freeze-bond shear stress τ_{FB}. a) saline water experiments b) fresh water experiments

In Figure 4 all salinities are displayed depending on submersion time. The salinity at 0.5 and 1 min was found to be stable at the level before submersion. For 5 - 60 min submersion times the salinity had a large variation between each sample. Samples submerged longer than 60 min had a clearly reduced salinity. The samples with initial temperature of -2.5°C generally had the lowest salinities.

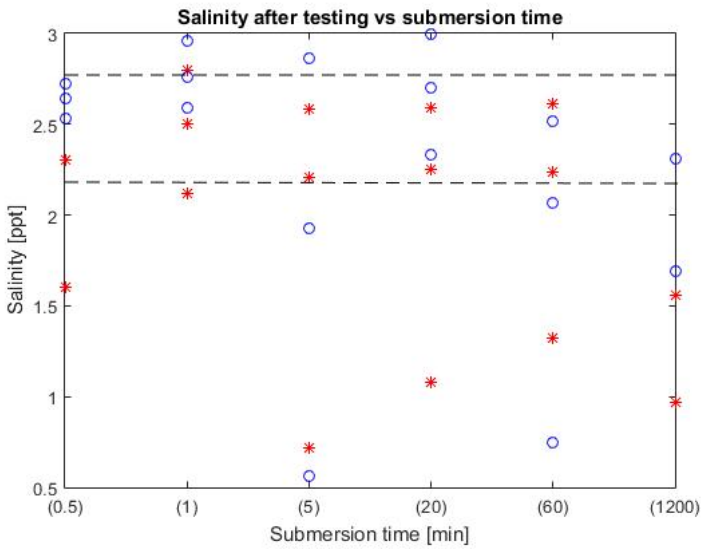

Figure 4. Salinity for all saline samples after testing sorted by submersion time. The red stars indicate initial temperature of -2.5°C and the blue circles -8.5°C. Span of initial salinity indicated by dotted lines.

Discussion

A bell-curve development of the stress described the stress dependency on submersion time. The fresh water samples generally peaked at shorter submersion times. A lower porosity in these samples increases the thermal conductivity. Air filled pockets also have a higher mass diffusion than brine filled pockets. This suggests that the potential energy will be transferred at a higher rate for fresh ice, causing the strength to peak at an earlier time. This trend agrees with the predictions of Shafrova and Høyland (2008), and the suggested driving forces, temperature and salinity, can be distinguished by that the fresh samples had a quicker first phase and a similar second and third phase development. The phases were described by Repetto-Llamazares et al. (2011).

The fresh water samples at -2.5°C were only strong enough to be tested for the shortest submersion times. The reduction in strength occurs quickly after reaching the peak strength. Why the strength did not stabilize as for saline samples and for the lower initial temperature remains unanswered.

The shear stress was higher for the lowest initial temperature, for both fresh and saline water. Shafrova and Høyland (2008) (initial temperatures from -1.8°C to -7.2°C) found the same trend for submerged fresh water samples, while Repetto-Llamazares et al. (2011) observed the opposite, increasing stress with increasing initial temperature as a clear trend, but only for the lowest confinement. Høyland and Møllegaard (2014) found that the stress was highest for the initial temperature of -8.5°C and lower for both -15°C and -2.5°C. The initial temperature has two effects on the freeze-bond stress. Firstly a lower initial temperature implicates that it takes longer before the sample reaches equilibrium with the submersion water, meaning it may be colder than the water during testing. This also affects

the brine content, faster ice growth locks in more brine. Secondly the speed of which the freeze-bonds form is higher. The strongest ice may be found at intermediate temperatures as suggested by Høyland and Møllegaard (2014).

The temperature development in the ice varied for the two initial temperatures. The samples at -2.5°C had a stable temperature for the submersion times of 0.5 and 1 min, before it started to increase. The samples at -8.5°C had increasing temperature from the shortest submersion time. The higher temperature gradient may explain the faster change. For both the temperatures the samples reached equilibrium with the water between 60 and 1200 min.

The saline samples increased in size during submersion while the fresh samples decreased. A redistribution of energy in the saline sample during warming, melting of ice in the sample releases energy which causes ice to form on the outside of the sample, explains this observation (Shestov and Marchenko, 2013). The salinity was measured both before and after testing. The salinity of the fresh water samples increased to that of the submersion water, which was still very low. For the saline samples the salinity decreased during submersion. This was assumed to result from brine drainage over time. This agrees with what was found by Møllegaard (2012), he measured the salinity of the freeze-bond specifically and found that it varied in the plane, more drainage towards the edges. In our experiments the freeze-bond section amounted to a relatively small area, making the drainage of brine a visible effect. For the intermediate submersion times of 5 - 20 min there were large variations in the salinity, this could indicate that drainage was on-going at this stage and reached equilibrium after 60 min.

The lowest salinities were measured for the highest initial temperature of -2.5°C for most samples. Likely this was due to the establish fact that faster ice growth locks in more brine. A lower salinity gives higher freeze-bond strength, but at the same time the lower temperature gives a higher strength. In general the samples with the lowest initial temperature had the highest freeze-bond strength. The initial temperature has a stronger influence on the peak stress than the salinity in these experiments.

Møllegaard (2012) found the peak stresses to be in a higher range than we found in this study. He used a similar test set-up, but the sample was longer (by 25 mm). We compared uni-axial samples at the two different heights it was found that the shorter sample gave lower freeze-bond stress. Shafrova and Høyland (2008) found peak stresses in the upper range for the uni-axial laboratory test. Ettema and Schaefer (1986), Repetto-Llamazares et al. (2011) Ettema and Shafer (1986) and Helgøy et al. (2013) studied the peak stress using direct shear tests. Their results were in the range 0.006 - 0.030 MPa, much lower than the tests with 45° set-up angle. This may be explained by an analysis in the τ-σ-plane, comparisons of the estimated cohesion and internal friction angle are presented in the next section.

THE τ-σ PLANE AND THE DERIVATION OF COHESION AND INTERNAL FRICTION VALUES

Results

The shear stress – confinement developments were studied. To describe the different developments 5 types were defined as listed below. The small sample basis limits the failure slope to be linear. With more samples the failure slope could show that a non-linear development would be appropriate. A least squares approach was used to estimate the failure slope.

1. Increasing shear stress with increasing confinement
2. Increasing shear stress with increasing confinement up to 0.020 MPa
3. Intermediate stress for the lowest confinement, lowest stress for the intermediate confinement and highest stress for the highest confinement
4. Highest stress for the lowest confinement, lowest stress for the intermediate confinement and intermediate stress for the highest confinement
5. Decreasing stress with increasing confinement

Most configurations were defined as type 1), these are the configurations used for calculating cohesions and internal friction angles. 6 out of 20 peak shear stress configurations and 14 out of 20 residual shear stress configurations had this development. The residual shear stress – confinement developments were more often defined as type 1), independent of the appertaining development type found for the peak stress.

The configurations in the 4 other categories may arise from premature failure. Three possible interpretations were considered. The first, a weakness in the sample, due to handling during testing or production. The second, a softening of the material. And the last that the radial confinement exceeded the strength of the freeze-bond, and it had already failed when the vertical compression was applied, this was observed only for the highest radial confinement. During testing when the radial force was applied we could hear the sample failing.

The interpretation of softening was looked into by estimating failure slopes from two samples and extrapolating it too the third sample. A line was fitted through the failure points of the samples with the two highest or the two lowest confinements. Assuming the first line to give an approximately correct tensile stress, this was used as a starting point for the second failure slope. If this assumption was suitable is unknown. The maximum difference in cohesion for the fitted and extrapolated line was 0.0054 MPa, which was in the order of 26.6 % lower. The internal friction angle was also in the same order less.

The third interpretation was tested by considering the ”failed” sample as a uni-axial test with the peak compression force equal to the set radial compression. It was then possible

to see if it crossed the estimated failure slope of the two other samples and if it failed before the test was started. This seemed appropriate for all configurations of this type. When plotted in this way it could be defined as a type 1) development and these failure slopes were also used for the estimation of cohesion values and friction angles, in total 13 of 20 peak stress configurations were defined as type 1).

Cohesion and internal friction angles have been calculated from estimated failure slopes of the peak shear stress – confinement developments and the residual shear stress – confinement developments. The results are presented in Tables 1 and 2 for the peak stresses and residual stresses accordingly. The configurations laying well above or below two times the standard deviation and the configurations giving negative cohesion values were excluded.

Table 1. Cohesion and friction angles for peak stress

	n	Mean cohesion (c)	SD c_{SD}	Mean friction angle (ϕ)	SD (ϕ_{SD})
Fresh configurations (all)	5	0.036	±0,017	30.93°	±5.69°
-2.5°C	1	0.028	±0	27.53°	±0°
-8.5°C	4	0.038	±0.019	31.74°	±5.85°
Saline configurations	8	0.028	±0.031	35.85°	±15.32°
-2.5°C	3	0.026	±0.021	33.90°	±15.31°
-8.5°C	5	0.028	±0.036	37.25°	±14.69°

Table 2. Cohesion and friction angles for residual stress

	n	Mean cohesion (c)	SD c_{SD}	Mean friction angle (ϕ)	SD (ϕ_{SD})
Fresh configurations (all)	5	0.007	±0,003	23.47°	±10.54°
-2.5°C	1	0.006	±0.002	23.18°	±8.10°
-8.5°C	4	0.008	±0.006	23.62°	±3.05°
Saline configurations	7	0.009	±0.006	25.03°	±10.00°
-2.5°C	3	0.006	±0.003	25.86°	±11.81°
-8.5°C	4	0.011	±0.006	24.40°	±7.85°

Discussion

Comparing the fresh and saline configurations, the mean cohesion values were found to be 30 % higher for the fresh than the saline samples for the peak shear stresses. For the residual stresses, the cohesion values were all close to zero as expected, but the saline gave somewhat higher values. The mean internal friction angles were higher for the saline configurations for both peak and residual stresses. This indicates that the stresses of the fresh samples were less influenced by increasing confinement.

Comparing the peak and residual stresses, the mean cohesion values were lower for the residual stress and the internal friction value lies in the lower part of the range of the peak stresses. The standard deviations were also found to be smaller for the residual stresses.

This would be expected from the assumption that the residual stress represents friction, which is less dependent on the small deviations between tests and between each sample.

A temperature dependency was also visible from the results. All mean cohesion values were higher for the lower initial temperature. Freeze-bonds have been found to have increasing strength for decreasing temperatures (Shafrova and Høyland, 2008), (Repetto-Llamazares et al., 2011), which would account for this finding. No obvious correlation was found between the cohesion/friction angle and the submersion time. A clear connection between the peak shear stress and the submersion time would be expected to be reflected in the cohesion and internal friction angle, a larger sample basis may give an answer to this.

The cohesion values were in the range 0.003 – 0.099 MPa and the internal friction 0.28 – 0.78 for the peak stresses. For the residual 0.001 – 0.018 MPa and 0.20 – 0.64. Repetto-Llamazares et al. (2011) found cohesion values in the range of 0.0014 – 0.0044 MPa and internal friction values in the range 0.19 - 0.59. Shafrova and Høyland (2008) extrapolated these results and compared them with their own, they fitted well. The results were in the same range as ours even though two different test set-ups were used, but a few configurations gave very high cohesion values in comparison. Schulson and Fortt (2012) found friction values in the range from 0.15 to 0.19 and cohesions from 0.0032 to 0.0056 MPa for sliding velocity of 1 mm/s and T_i = -10°C. The friction coefficients fits with the lower range of our residual friction angles, and their cohesions are somewhat less than what we found, but still close to zero.

CONCLUSIONS

The freeze-bond stresses were found to be in the same range for the uni-axial samples as found for previous experiments. The freeze-bond stress dependency of submersion time, initial temperature and salinity was all found to reinforce the existing theory. This gave a good basis for studying the effect of radial confinement.

Both our results and results from earlier similar set-ups (sample loaded 45° to the freeze-bond orientation) gave higher peak shear stresses than direct shear experiments. This can be explained by the introduction of Mohr-Coulombs failure criterion. We found values in the range 0.003 – 0.099 MPa for cohesion and 16 – 45° (0.28 - 0.78rad) for internal friction for the peak stresses. For the residual stresses the cohesion values were approaching zero and internal friction angles were in the range 11 – 37° (0.19 - 0.65rad). The estimated cohesion and friction values were in the same range and in agreement with earlier measurements, no clear difference was found between the direct shear tests and the tests with a set-up angle.

Comparing the fresh with the saline configurations the mean cohesion values were found to be 30 % higher. The mean internal friction angles were higher for the saline configurations. A dependency on initial temperature was also seen by the cohesion values, higher cohesion for the lower initial temperature of -8.5°C.

The fresh ice had only strong enough freeze-bonds for short submersion times at the initial temperature of -2.5°C. How the freeze-bonds disintegrates we do not know.

ACKNOWLEDGEMENT

We wish to acknowledge Aleksey Shestov and Jomar Finseth for their contributions to conducting the experiments. We also wish to acknowledge the support from the Research Council of Norway through the Center for Research-based Innovation SAMCoT and the support from all SAMCoT partners.

REFERENCES

Ettema, R., Schaefer, J., 1986. Experiments on freeze-bonding between ice blocks in floating ice rubble. Journal of Glaciology 32 (112), 397–403.

Helgøy, H., Skog Astrup, O., Høyland, K. V., 2013. Laboratory work on freeze-bonds in ice rubble, part 1: Experimental set-up, ice-properties and freeze-bond texture. Port and Ocean Engineering under Arctic Conditions.

Høyland, K. V., Møllegaard, A., 2014. Mechanical behaviour of laboratory made freeze-bonds as a function of submersion time, initial ice temperature and sample size. 22nd IAHR International Symposium on Ice.

Møllegaard, A., 2012. Experimental study on freeze-bonds in laboratory made saline ice.

Repetto-Llamazares, A. H., Høyland, K. V., 2011. Review in experimental studies on freeze-bonds. In: Proceedings of the International Conference on Port and Ocean Engineering Under Arctic Conditions. No. POAC11-021.

Repetto-Llamazares, A. H., Høyland, K. V., Evers, K.-U., 2011. Experimental studies on shear failure of freeze-bonds in saline ice: Part I. Set-up, failure mode and freeze-bond strength. Cold Regions Science and Technology 65 (3), 286–297.

Schulson, E. M., Fortt, A. L., 2012. Friction of ice on ice. Journal of Geophysical Research: Solid Earth 117 (B12).
URL http://dx.doi.org/10.1029/2012JB009219

Shafrova, S., Høyland, K. V., 2008. The freeze-bond strength in first-year ice ridges. small-scale field and laboratory experiments. Cold Regions Science and Technology 54 (1), 54–71.

Shestov, A., Marchenko, A., 2013. Thermodynamic consolidation of ice ridge keels in water at varying freezing points. Norwegian University of Science and Technology.

Appendix

Freeze-bond shear strength calculation

$$A_{ellips} = \sqrt{2}\pi r^2 \tag{4}$$

$$A_{circ} = \pi r^2 \tag{5}$$

$$h = \frac{2r}{\pi}\theta \tag{6}$$

$$\sigma_z = \frac{Measuredpistonforce}{A_{circ}} \tag{7}$$

Force from σ_r in x-direction:

$$\begin{aligned} F &= -2\int_0^{\pi} \sigma_r h(\theta) r cos(\theta) d\theta \\ &= -2\sigma_r \frac{2r}{\pi} r \int_0^{\pi} \theta cos(\theta) d\theta \\ &= -K[\pi * 0 + cos\pi - (0 * 0 + cos0)] \\ &= -K[+(-1) - (1) = 2K \\ &= 8\sigma_r \frac{r^2}{\pi} \end{aligned} \tag{8}$$

Sum of forces in z-direction:
$\sum F_z = 0$

$$\begin{aligned} \sigma_z \pi r^2 - \frac{\sqrt{2}}{2}\tau_{FB}\sqrt{2}\pi r^2 - \sigma_{FB}\frac{\sqrt{2}}{2}\sqrt{2}\pi r^2 = 0 \\ \sigma_z - \tau_{FB}\sigma_{FB} = 0 \\ \tau_{FB} = \sigma_z - \sigma_{FB} \end{aligned} \tag{9}$$

Sum of forces in x-direction:
$\sum F_x = 0$

$$\begin{aligned} 8\sigma_r \frac{r^2}{\pi} + \frac{\sqrt{2}}{2}\tau_{FB}\sqrt{2}\pi r^2 - \frac{\sqrt{2}}{2}\sigma_{FB}\sqrt{2}\pi r^2 = 0 \\ \frac{8}{\pi}\sigma_r + \pi\tau_{FB} - \pi\sigma_{FB} = 0 \\ \sigma_{FB} = \frac{8}{\pi^2}\sigma_r + \tau_{FB} \end{aligned} \tag{10}$$

Equation 9 in equation 10

$$\begin{aligned}\sigma_{FB} &= \frac{8}{\pi^2}\sigma_r + \sigma_z - \sigma_{FB} \\ &= \frac{4}{\pi^2}\sigma_r + \frac{1}{2}\sigma_z \\ \tau_{FB} &= \sigma_z - \frac{4}{\pi^2}\sigma_r - \frac{1}{2}\sigma_z \\ &= \frac{1}{2}\sigma_z - \frac{4}{\pi^2}\sigma_r\end{aligned} \tag{11}$$